Sensing and Actuation: Lunar Zebro Rover Deployment System

Bachelor Graduation Thesis

N. Kant
T. J. Velzel

Delft University of Technology

TU Delft

LUNAR ZEBRO

Sensing and Actuation: Lunar Zebro Rover Deployment System

by

Noa Kant & Tadjiro Velzel

Noa Kant	5402638
Tadjiro Velzel	5229642

Project Supervisor:	Prof. C. J. M. Verhoeven
Project Duration:	April - June, 2024
Faculty:	EEMCS, Delft

Cover:	Lunar Zebro Render (Modified)
Style:	TU Delft Report Style, with modifications by Daan Zwaneveld

TU Delft

Abstract

The Lunar Zebro rover is a nano rover designed by student research team Lunar Zebro at the Technical University of Delft. This rover will be sent to the lunar surface to conduct scientific experiments. In order to protect the rover during transit and facilitate successful deployment onto the lunar surface, a rover deployment system was designed.

This thesis describes the design of the sensing and actuation part of the rover deployment control system. The thesis details the design of a system which is able to deploy 4 Non-Explosive Actuators by means of sequentially supplying more than 4A for 50ms to each NEA. This sequence is inhibited by a physical connection to the rover by means of an umbilical cord which can be overridden when the rover and microcontroller send an override signal at the same time. The system contains a heating element and two temperature dependent relaxation oscillators that can be used to regulate the temperature. Thermal regulation can function independently of a digital control system, but can also be managed by the microcontroller. In the case that the microcontroller experiences failure, the NEA activation sequence can be initiated by two control signals from the lander, to which the deployment system is attached.

The system has not been physically tested, but has been verified in simulation. The combination of all these subsystems uses a peak power of 1.1W in simulation.

A test printed circuit board was designed to incorporate the complete rover deployment control system. This board can be used to physically simulate the deployment of the four non-explosive actuators by means of glass fuses. The board also allows any equivalent NEA model to be used in order to verify the limits of the system.

The system meets all functional requirements in simulation. Future work regarding the design entails physical testing of the PCB and the resolution of two major vulnerabilities, namely its reliability on the stability of the lunar lander's 28V supply as well as its inability to handle excessive thermal energy.

Preface

The Lunar Zebro Rover is a nano rover developed to operate on the lunar surface. The Lunar Zebro team aims to send the rover as a piggyback payload on a lunar lander. During transit to the moon, the rover is protected by the rover deployment system, which subsequently releases the rover after making contact with the lunar surface. The rover deployment system requires an electrical control system to relay information between the lander and the rover during transit. Furthermore it allows the rover's battery to be maintained at a suitable state of charge. Lastly, it facilitates the deployment sequence onto the lunar surface by activating four non-explosive actuators.

The design of the complete rover deployment control system was subdivided into three parts. Each part of the design was developed by a separate subgroup. The first group was tasked with designing the communications and digital control system. The second group was appointed to the design of the internal power system. The third group was tasked with developing the sensing and actuation elements of the control system. The design of the sensing and actuation elements will be detailed within this thesis.

The design project was commissioned by the Lunar Zebro student research team, who require this system in order to achieve mission success. The development of the rover deployment control system was supervised by Chris Verhoeven.

Noa Kant & Tadjiro Velzel
Delft, July 2024

Contents

Nomenclature

List of Abbreviations

Abbreviation	Definition
RDS	Rover Deployment System
NEA	Non-Explosive Actuator
LZ	Lunar Zebro
CS	Control System
MCU	Microcontroller unit

1

Introduction

Lunar Zebro is ”World’s smallest and lightest rover yet, built by TU Delft students” [1]. The focus of the Lunar Zebro team is sending the rover to the moon as a piggyback payload, which is attached to a lunar lander. After the lander makes contact with the lunar surface, it will send a signal indicating that the Rover Deployment System (RDS) should release the rover onto the lunar surface. Thus, the primary goal of the RDS is to release the rover onto the lunar surface upon receiving a deployment signal. The rover must not be released at any other moment.

During the early stages of RDS development, the need arose for an electrical system that controls the mechanical system, allows the rover to communicate with the lander, and provides power from the lander to the rover. This functionality is crucial to the success of the entire mission, indicating the critical role of the RDS electronic subpart.

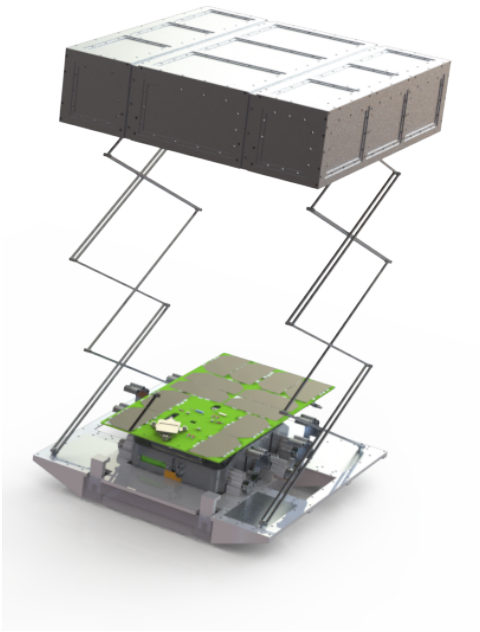

Figure 1.1: Rover Deployment System

1.1. State-of-the-Art Analysis

Space exploration started in 1957 and has since grown into a 630 billion dollar industry [2]. Large agencies such as NASA and ESA are developing various projects to extend human knowledge about extraterrestrial life. These agencies develop products with similar goals as the Lunar Zebro rover, such as nanosatellites, which also weigh between 1-10 kg and operate in the same harsh environments[3]. These nanosatellites are deployed into space to orbit in the Low Earth Orbit zone, which lies between 200 to 2,000 kilometres above Earth. The product most similar to the Lunar Zebro RDS is the deployment system used for these nanosatellites. An example would be the ISIPOD CubeSat Deployer, created by ISISPACE [4]. However, very little information about their control systems is publicly accessible. Many space agencies maintain large amounts of proprietary information, which makes it difficult to find information about their electrical control systems.

1.2. Purpose and Scope

The goal of the Rover Deployment System is to deploy the Lunar Zebro rover to the surface of the moon, as written in the system overview (Chapter 2). Non explosive actuators have been used in state of the art space applications such as the release of the solar panels, primary and secondary mirror

assemblies of the James Webb Space Telescope [5]. However, they have never been used to deploy a vehicle to the lunar surface. Therefore, methodical development of this system is crucial to the success of the Lunar Zebro mission.

The success of the mission depends on the RDS' ability to withstand the harsh environment of space, including temperatures ranging from -170 to 130 degrees Celsius [6], high acceleration during transport and low amounts of available power. Furthermore, the large cost of transporting mass to the lunar surface, and Lunar Zebro's future ambitions towards robotic swarming, underline the need for a lightweight system. Therefore, developing the RDS control system not only requires a combination of expertise in low power engineering, electronics design, and embedded systems, but also requires extensive knowledge of robust, reliable, and lightweight design.

Lunar Zebro aims to launch their rover at the end of 2025. Considering this system is crucial in order to achieve mission success, there is high urgency for a first draft design, which can subsequently be optimised and certified.

1.2.1. Stakeholders and Users

The main stakeholder for this project is the Lunar Zebro student research team, as this team provides the context in which the project takes place. The insights and methodologies developed here could be used as a basis for future Lunar Zebro projects and contribute to the broader field of electronic systems for space deployment mechanisms. Other major stakeholders are also the other two bachelor project teams working on the rest of the RDS control system, as clear communication between these groups is essential for a good design.

Another stakeholder is the company responsible for the lunar lander. As the Lunar Zebro mission is a piggyback mission, it is important that the design is cleared before it is launched. It is therefore important the design achieves the necessary certifications. However, which lunar lander will be used for the definitive launch is unknown during this project.

1.3. Thesis Synopsis

This thesis will cover the sensing and actuating subsystems of the RDS control system. This includes current sensors to check internal power flows, temperature sensors for thermal control of the RDS, sensors to monitor actuator status, and most important of all: the activation system of the actuators that will release the rover. These elements are integrated within the complete electronic RDS and implemented on a printed circuit board (PCB). The design of this PCB is also covered within this thesis.

This thesis will make use of control signals from a microcontroller and different voltages. The programming of the microcontroller and the conversion of the lander's power supply to the systems' different voltages are outside the scope of this thesis, as these elements are designed by different sub-groups.

2

System Overview

The Rover Deployment System was designed with three objectives:

1. Deploy the Lunar Zebro rover on the surface of the moon.
2. Provide power from the lander to the rover during transit when needed.
3. Function as an intermediary for communication between the rover and the lander.

In order to achieve these objectives, the electronic RDS contains a number of subsystems. An overview of these subsystems and their interactions is shown in Figure 2.1. This thesis covers elements of the RDS relating to actuation and sensing. These elements are portrayed in red within the figure. Elements for which their details fall outside the scope of this thesis are shown in black.

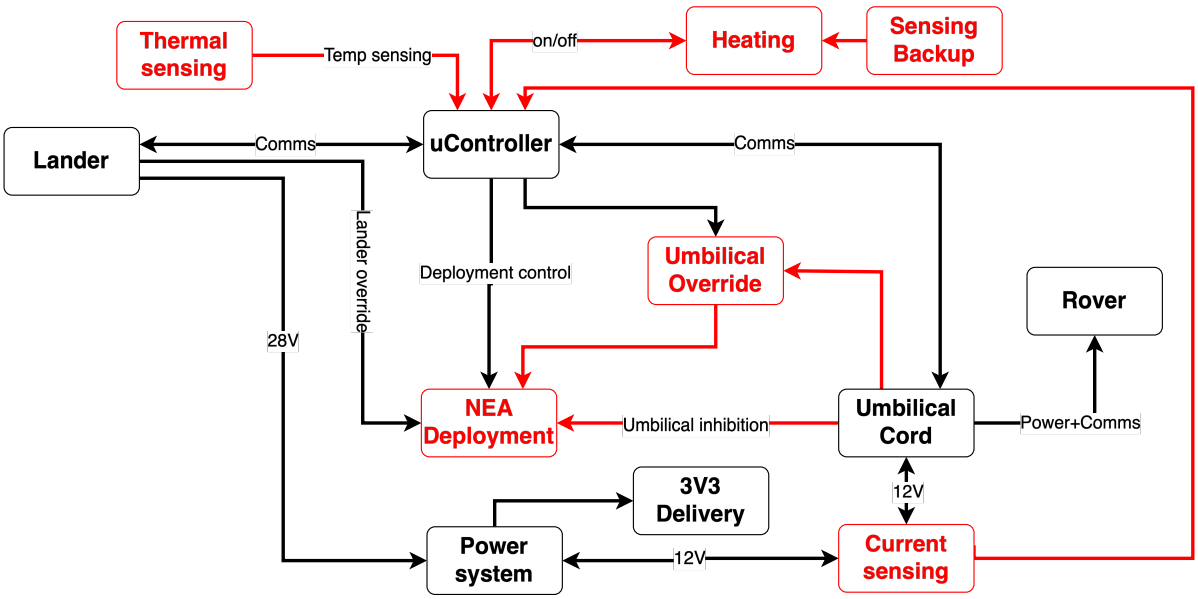

Figure 2.1: System overview

The deployment of the rovers will occur with Non-Explosive Actuators (NEAs): components that push or pull a pin once a sufficiently high current has been driven through them for a specific time. The deployment of the Non-Explosive Actuators and the sensing thereof are detailed in this thesis, as well as the umbilical inhibition and override system.

The thermal regulation system includes thermal sensing, backup sensing, and the capability to heat portions of the RDS. This is part of the set of sensing and actuation elements within the RDS, and will

therefore be covered in this thesis.

A test PCB has also been designed. This PCB has been created by the authors of this thesis. Therefore, its design will also be covered in this thesis.

A Microcontroller Unit (MCU) is used for the RDS. It serves as a system controller and communication passthrough: it sets control signals high or low based on measurement inputs, and passes communication from the lander to the rover and vice versa. The microcontroller is programmed by a different group. The architecture of the control system as implemented within the microcontroller will therefore be covered in a different thesis [7].

The design of the power system is done by a third group [8]. This power system will convert the 28V supplied by the lander to 12V for the Rover power supply. This group also provides the circuitry necessary to supply 3.3V to the microcontroller.

An umbilical cord is used to relay communications and power: a physical connection between the RDS and the Rover. This umbilical cord has not yet been selected, but a market analysis of available off-the-shelf components shows that umbilical cords with 6 or more connections are not outside the norm. In this design, 6 connections will be assumed. The selection of a specific umbilical connector is outside the scope of this thesis. More info can be found in the power system report [8].

3

Programme of Requirements

3.1. Requirements Overview

3.1.1. Functional requirements

The elements covered within this thesis have the following functional requirements.

1. The system must be able to actuate 4 Non-Explosive Actuators [1]
2. The NEAs must not activate before the rover is ready for deployment
3. The system must activate the NEAs when the rover is ready for deployment
4. The system must be able to actuate the 4 NEAs within 120 minutes

3.1.2. Non-functional requirements

The system as described within this thesis has the following non-functional requirements.

1. An umbilical cord must be used to connect the RDS to the Rover
2. The system should be able to operate after being exposed to temperatures between -120 and +120°C
3. The system must be able to deploy the NEAs within the entire rated temperature range of the NEAs, from $-60°C$ to $120°C$.
4. The system should be able to withstand 6g of constant acceleration, and 9g of peak acceleration.
5. The system should be able to operate on 3W, 28V DC supply.
6. The system must be able to deploy the NEAs in a vacuum.

3.1.3. Trade-off Requirements

The system also specifies two trade-off requirements, indicating priority goals that should always be kept in mind, but may be overridden when the design demands it.

1. The rover deployment control system must weigh less than 200 grams
2. The rover deployment control system must be smaller than 20cm x 20cm x 10cm

[1] The specific type of NEA and its characteristics are specified in Section (4.1

4

Design Considerations

This chapter discusses a number of relevant design considerations relating to components that are commonly used in design for space applications. Suitable components are evaluated for their ability to withstand temperature swings and exposure to vacuum. Furthermore the characteristics of the NEAs are discussed.

4.1. Designing for NEAs

The design of the actuation system assumes that the chosen model of non-explosive actuator is either the EBAD 1120-05 [9] or the EBAD 9040 [10]. These options have weight- and loading characteristics suitable for the deployment system. The product datasheets specify that these products require at most 4A of current for 50ms to deploy [9]. The extensive testing of NASA's JWST team with the EBAD 9102 shows the graph in Figure 4.1 representing the current and time required to deploy the device at ambient conditions. Furthermore, the JWST research team found that 9 different EBAD 9102 models

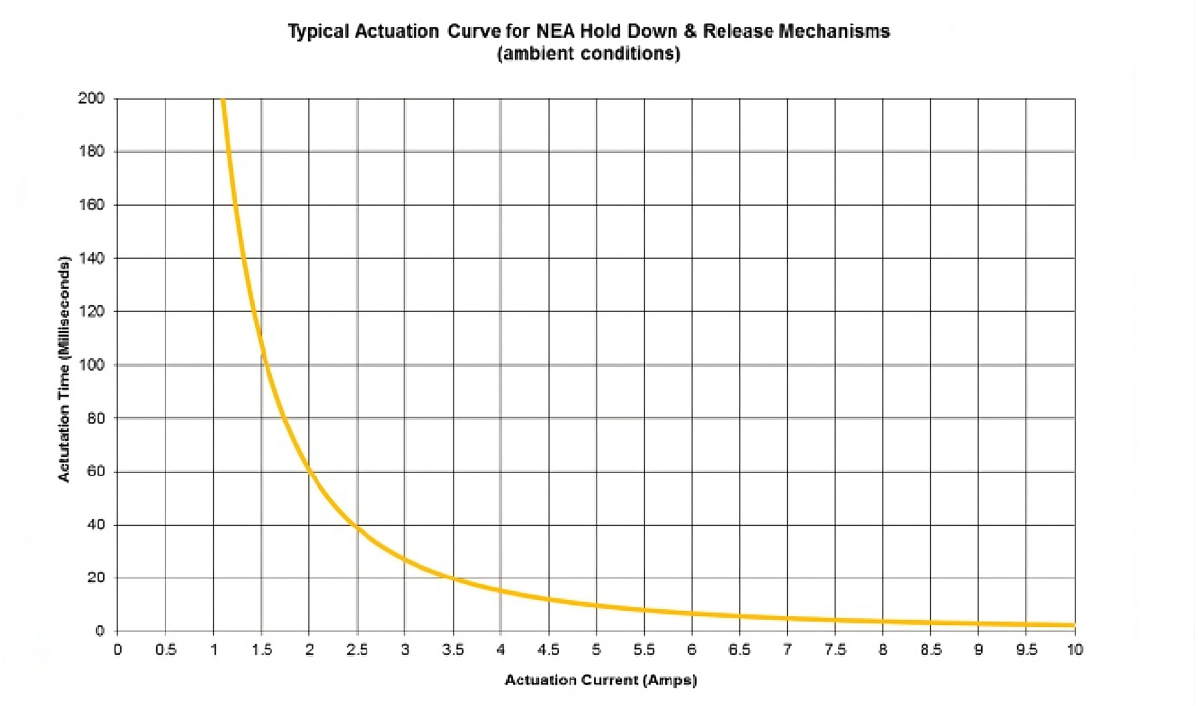

Figure 4.1: Current and time needed to deploy EBAD 9102 at ambient temperature. Taken from [11]

deployed within 40ms, using 3A during thermal vacuum testing at 28 Kelvin [5]. The product sheet

Device	Ebad 9040	Ebad 1120-05
Weight	13.6g	45g
Electrical resistance	$1.3 \pm 0.5\Omega$	$1.3 \pm 0.3\Omega$
No-Fire Current	250mA	210 mA
Operational Temperature Range	-60 to 125 ° C	-51° to 172 ° C
Actuation current	3.0A for 50ms	4.0A for 25ms

Table 4.1: Summary of Ebad NEA characteristics

specifies that the NEA will never deploy when a continuous current up to 250mA is supplied. The characteristics of both models are summarised in Table 4.1.

Considering the significant price of even a single NEA, the authors decided to simulate it by using glass fuses. The widespread availability of glass fuses allows for testing with different maximum currents, allowing extensive testing of the system. Because the NEAs are so costly, it was not possible to measure qualities such as the inductance and capacitance of the device.

4.2. Component Selection

In space applications, there are some limitations that are not relevant for terrestrial applications. These mainly consist of the wide temperature range encountered, the vacuum of space, and the strong background radiation present in space.

In the design of the RDS control system, the background radiation is of lesser importance. This is due to the fact that the pod in which the control system and the rover are transported will not only protect from debris, but also from background radiation, as it functions as a Faraday Cage.

The lack of atmosphere, besides making certain components impossible to use, makes temperature dependency a bigger issue. Due to the lack of air, components can no longer make use of convection, and can only conduct heat through connected surfaces or radiation.

4.2.1. Resistors

Resistors with large temperature-independence are widely available [12]. If resistors are used for voltage division, the only relevant factor is that their temperature dependence is identical. This implies that the ratio between the two resistor values is constant.

4.2.2. Inductors

Inductors are often made of copper windings. The resistance of copper decreases with decreasing temperature, thus the losses caused by the inductors resistance will also decrease with temperature. Some inductors available on the market are rated to withstand temperatures from -200 to +150 degrees Celsius [13], which makes them suitable to space applications.

4.2.3. Capacitors

Ceramic capacitors are nearly temperature independent, and have been shown to have a negligible difference in capacitance when tested down to -200 degrees Celsius [14]. Electrolytic capacitors can also be used [15], but are not as temperature stable as ceramic capacitors [14].

4.2.4. Transistors

In doped silicon, the voltage to current relation follows the equation

$$J = J_s e^{\frac{eV}{kT}-1} \tag{4.1}$$

[16]. This relation is thus quite temperature dependant, and transistors based upon the PN junction thus fare relatively poorly under low temperatures. It is better to use MOSFETs, as the field effect is less dependent on temperature [17].

4.2.5. Diodes

For the same reasons as with transistors explained in the section above, it is best to avoid diodes based on the PN junction. Schottky diodes are not based upon this junction, and usually have a lower voltage clip. They are thus preferable to use.

4.3. PCB Design

There are a number of concerns regarding the change in mechanical and electrical characteristics of printed circuit boards (PCBs) in space. These concerns relate mostly to the lack of air pressure and the variation in temperature. PCBs usually make use of their larger surface area to dissipate heat to the surrounding air. This lack of convective dissipation and the subsequent buildup of thermal energy can lead to significant thermal expansion and contraction of elements connected to the PCB, potentially causing failure of solder joints and other connections. Excess thermal energy, when conducted to connected elements, can also change their electrical properties.

Certification of PCB materials regarding thermal characteristics is usually classified by 'Tg rating', indicating the glass transition temperature. There are many materials available with a high Tg rating, such as cyanate ester, featuring a glass transition temperature of above 220 $^{\circ}$ C.

5

Failure Tree

The requirements and limitations of the system intuitively lead to a possible implementation of the actuation circuit. This circuit would include a current source, an inhibitory system - which prevents the NEA from activating at the wrong time-, the NEA itself, and an activation system. A graphic of such a system can be found in Figure 5.1.

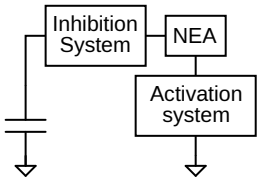

Figure 5.1: Possible implementation of system

This initial idea leads to a structure in which there are two controlling elements. A prime candidate for a control signal to drive the inhibiting circuit is the connection of the umbilical cord. As long as umbilical cord is connected, the inhibiting system prevents NEA deployment. In order to coordinate the communication, charging and actuation functionality within the rover deployment system, a microcontroller is used. This microcontroller forms the second controlling element, driving the activation system. Assuming no other components or systems fail, this situation leads to the failure tree in Figure 5.2.

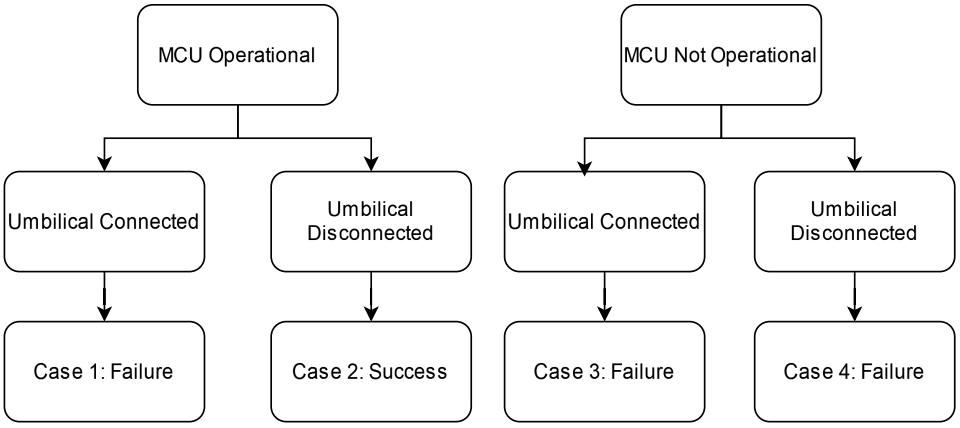

Figure 5.2: Failure tree using two separate controlling elements

This tree has a case during which deployment could be attempted by the microcontroller even if the umbilical cord is still disconnected. Allowing the microcontroller to single handedly override the umbilical

cord only shifts the failure cases around, instead of removing them, as it allows a malfunction of the microcontroller to cause a failure in a situation for which the umbilical cord inhibition system would otherwise prevent a misfire. A more effective approach could be to make use of the controlling elements that are currently uninvolved in the actuation sequence. One option for this role can be the rover itself. Combining the controlling elements of the rover and microcontroller enables the design of an override system, in which the override is not dependent on a single point of failure. In the case that the rover and MCU are both operational, this system could turn ”Case 1” of Figure 5.2 into a success by overriding the umbilical inhibition system.

In order to turn case 3 and 4 into a potential success, a more rigorous approach is needed. The communication structure of the system, as shown in Chapter 2, causes the rover to be cut from all lander communication if the microcontroller experiences failure. In the case that the rover could initiate the deployment during microcontroller failure, it would have to deploy blindly, as it cannot retrieve information from the lander.

A safer approach would be to involve the lander as a controlling element. Deployment through the lander would have to be driven by simple signals, as there is no digital infrastructure operating to interpret them. The lander has no information on the output of sensors on the RDS such as the state of charge of the capacitor or the battery of the rover, and should therefore only be used as a last resort to push the rover onto the surface, without knowing if its batteries are charged. Using the lander to deploy the rover would turn all four cases of Figure 5.2 into a success. However, it could conflict with functional requirements, such as mandatory requirement 2: ”The NEAs must not activate before the rover is ready for deployment”, as stated in Chapter 3.

6

System Design

6.1. NEA Actuation

Activating the Non-Explosive Actuators (NEAs) at only the appropriate time is the most important element of the entire Rover Deployment System. Great care must be taken that the system does not deploy before it should. This section discusses how the system is designed to prevent precocious deployment and activate the NEAs at the appropriate time.

6.1.1. High- and Low-side Switching

The NEA activation circuit makes use of both high- and low-side switching. This subsection will discuss the advantages and disadvantages of both topologies and the design decisions that were based thereon.

Low side switching involves a switch between the load and ground. This configuration commonly makes use of an n-channel MOSFET. High side switching places the switch between V_{dd} and the load, commonly using a p-channel MOSFET. This difference is illustrated in Figure 6.1.

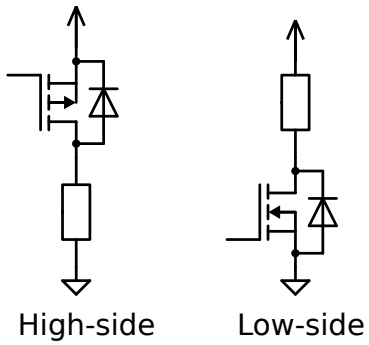

Figure 6.1: High-side and low-side switching

When an n-channel MOSFET, of which the source is connected to ground, experiences a potential of $0V$ at its gate, V_{gs} is assumed to be far below V_{th}, indicating that the device is not conducting from drain to source. In the case of a p-channel MOSFET experiencing a gate potential of $0V$ and $V_{DS} >> V_{th}$, the opposite is true. In this case, the source is connected to V_{dd}, meaning that V_{gs} is the same as V_{dd}. This indicates that the p-channel MOSFET is effectively conducting between its source and drain terminals.

This difference in reference has important implications in case of a power system failure. In the case that a system using a p-channel device, which inhibits a capacitor from discharging, undergoes power system failure, the MOSFET could no longer prevent the capacitor from discharging. Similarly, if a

system using an n-channel MOSFET suffers from power loss, it is no longer able to initiate the discharge sequence.

Low side switching allows for a simpler gate drive circuit, as the source is at ground potential. Subsequently, driving the device requires lower voltages as the operation of the switch is dictated by the gate voltage relative to ground. As the source of a p-channel MOSFET is usually connected to V_{dd}, higher voltages are needed to push the device into saturation mode.

Because V_{GS} is in reference to V_{dd}, the gate drive circuitry is more complex, because the source is not at a fixed potential. The differences in the complexity of gate drive circuitry are reflected by the cost and availability of gate driver ICs, showing that there are fewer options for high-side switching driver ICs. The options that are available are usually more costly than low-side switching driver ICs.

One way of assessing the stability of a MOSFET is by evaluating the amount of connections to other components at the drain and source. For low-side switching, the source is connected to ground. As there are usually many components connected to a common ground, which can all cause instability of the ground reference, low-side switching is less effective in applications that require stable V_{DS}. The same can be said for high-side switching, when many components are connected to a common V_{dd}.

Lastly, some applications use either ground or V_{dd} as a reference for their operation and cannot function properly if a component with non-negligible resistance is placed between the device and ground. One such example is the relaxation oscillator used to determine the temperature within the RDS, as described in Section 6.4.

6.1.2. Capacitor Activation

The umbilical inhibitor uses high-side switching, while the MCU sends the NEA activation signal to a low-side switch. A high-side switch was chosen such that the NEAs are isolated from the supply voltage in case of a short to ground in the activation circuit. A low-side switch was chosen such that the NEAs do not activate in case of a power system failure. The combination of these two ensures effective isolation of the NEAs, preventing an accidental actuation in case of a common failure. This was identified as a sufficiently significant advantage to outweigh the added complexity from using both types of switching. As this is an application which does not require a very stable ground reference, the stability concerns surrounding low-side switching are not applicable here.

6.1.3. Capacitor Charge Level Sensing

The NEAs should only be activated once the capacitor is sufficiently charged to fully deploy a NEA. It is therefore important that the MCU can read the level of charge of the capacitor. This is done via a resistive divider to ground, where the 0-28V range of the capacitor charge is scaled to a 0-3.2V range. As the microcontroller has an internal ADC, this signal can be directly fed to the microcontroller. A transient voltage suppression (TVS) diode has also been added to protect the microcontroller terminals from receiving voltages that could damage the microcontroller. The setup is pictured in Figure 6.2, and is used everywhere a voltage is sensed by the microcontroller.

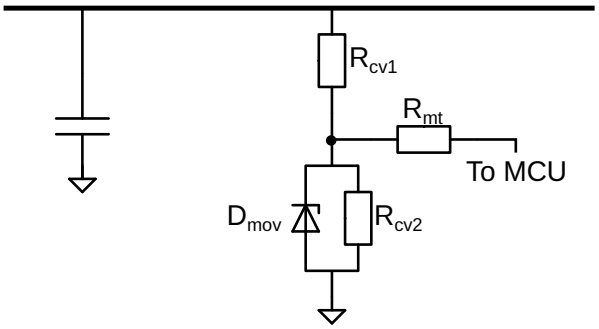

Figure 6.2: Capacitor voltage sensing: used anytime a voltage is sensed to the MCU

The component values as shown in Table 6.1 have been chosen in the final design for this configuration.

R_{cv1}	$120k\Omega$
R_{cv2}	$15k\Omega$
R_{mt}	$1k\Omega$
D_{mov}	D1213A-01T

Table 6.1: Component values for capacitor charge level sensing

6.1.4. Umbilical Inhibition

The status of the umbilical cord, connecting the rover to the RDS, is used as a controlling element for the NEA activation circuit. Herein, a p-channel MOSFET is kept in cutoff mode as long as the umbilical cord is connected. The status of the connection is evaluated electrically by means of a 12V line originating from the rover's internal power system. This signal is also used as a control signal for the MCU, in the way described in Section 6.1.3.

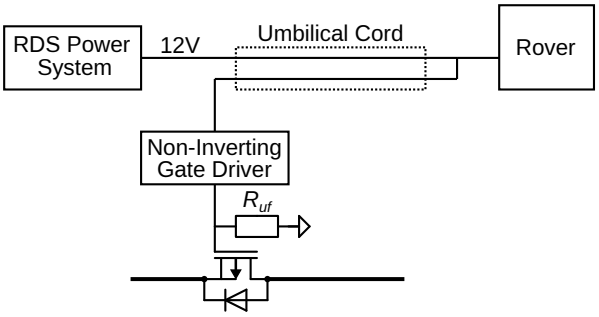

Figure 6.3: The umbilical connection check originates on the rover's side of the umbilical cord

6.1.5. Umbilical Inhibition Override

Section 5 describes how adding an override on the umbilical inhibition system has the potential to turn a failure case into a success. This can be achieved by allowing the microcontroller and the rover to override the inhibition system when both raise an override flag.

The inhibition system should be active when the umbilical connector is still attached, and when the rover and microcontroller do not both raise their override flags. This leads to the logic configuration as shown in Table 6.2, wherein A indicates the umbilical connector is attached, whereas A' indicates it is disconnected. B indicates the microcontroller has raised its override flag, whereas B' indicates it has not. The same situation applies for C, which indicates the rover has raised its override flag, whereas C' indicates it has not. An output of '1' indicates the inhibition system is active, whereas a '0' indicates it should be overridden.

-	B'C'	B'C	BC	BC'
A	1	1	0	1
A'	0	0	0	0

Table 6.2: Table indicating when the inhibition system is active, A corresponds to an attached umbilical cord, whereas B and C indicate the microcontroller and the rover's override flags respectively.

Considering a p-channel MOSFET is not conducting when a sufficient positive voltage is applied with reference to the source voltage, the logic function in Equation 6.1 needs to be applied to the gate of the MOSFET.

$$AB' + AC' = A(B' + C') \tag{6.1}$$

This is equivalent to applying the logic function of Equation 6.2 to the input of an inverting gate driver.

$$(A(B' + C'))' = ((BC)'A)' \tag{6.2}$$

This function can be implemented using two NAND gates, leading to the implementation of Figure 6.4. Note that there is a connection to ground from the gate terminal of the MOSFET through a resistor,

ensuring that if the gate driver's connection to the gate experiences failure, the MOSFET will continue to conduct.

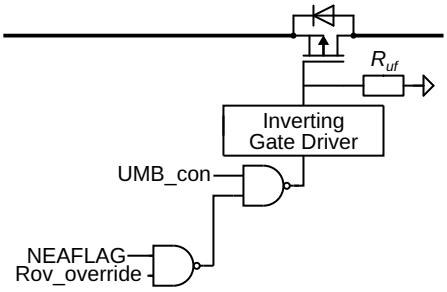

Figure 6.4: Implementation of the umbilical override system

The complete circuit is implemented by means of the components as in Table 6.3

R_{uf}	$1M\Omega$
Inverting Gate Driver	FAN3278
Dual Circuit NAND	SN74LVC2G132DCTR
P-channel MOSFET	FQA9P25

Table 6.3: Component values for umbilical inhibition system

6.1.6. Use of Gate Drivers

Circuits involving resistances, capacitances and inductances have a tendency to oscillate when they are excited. Similarly, MOSFET devices can exhibit oscillations, wherein the type and frequency of the oscillation depends on the excitation method and parasitics in the circuit. This section discusses the effects and prevention of oscillations at the MOSFET's gate.

In the case of our design, oscillations are worsened primarily by two factors: parasitic capacitance and parasitic inductance. Parasitic inductances are caused by the component leads and the traces of the circuit. These inductances interact with capacitances in the load and MOSFET body to cause parasitic oscillations. These oscillations can cause large overshoot voltages, which can damage both the load and the MOSFET itself.

MOS devices may lower their conduction resistance R_{ds} when the Gate-to-source voltage V_{GS} is increased. As V_{GS} is increased however, the electric field across the gate oxide may become too strong, causing breakdown of the oxide layer. This phenomenon is referred to as 'Gate Oxide Breakdown'. Gate oxide breakdown results in a permanent short circuit between the gate and channel, meaning the gate loses its ability to control the channel [18]. Therefore, increasing V_{GS} may improve the device performance but also increases its susceptibility to gate oxide breakdown caused by voltage overshoot in the case of parasitic oscillations at the gate of the device. An example of oscillations visible at the gate of a MOSFET is visible in Figure 6.5.

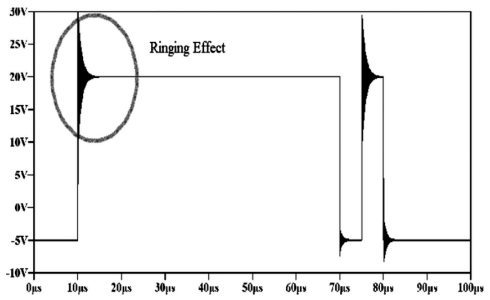

Figure 6.5: Oscillations at the gate of a MOSFET device in an automotive power converter, showing significant voltage overshoot. 2020, Murugesan et al [19].

In order to minimise the risk of gate oxide breakdown, a gate driver can be used. The gate driver limits the gate voltage by suppressing oscillations and limiting the DC voltage. Gate drivers can also improve performance by quickly pushing the device into either cutoff or saturation mode. This reduces the period during which the device is dissipating large amounts of energy while operating in linear mode. In the interest of avoiding single points of failure, the gate driver can be bypassed by the lander override system, as described in Section 6.3. The complete schematic including the gate drivers, their input logic and the MOSFETs' standard modes are visible in Figure 6.6.

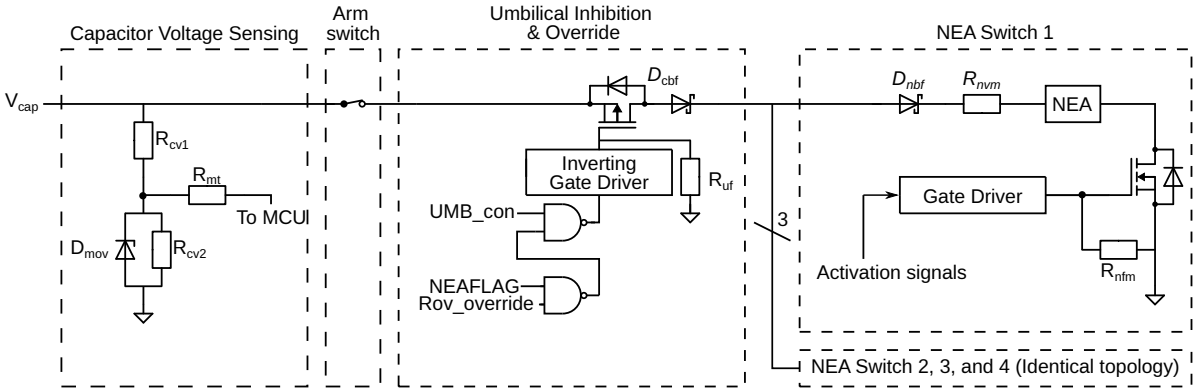

Figure 6.6: Complete design of NEA activation system

6.2. NEA Sensing

The level of coordination of the activation of the NEAs can be greatly improved by introducing a sensing mechanism to evaluate whether each NEA has been successfully deployed. This sensing mechanism should work independently of the state of the inhibition and activation mechanisms, as well as the state of charge of the capacitors. Therefore, the system must operate with a varying voltage source, a varying high side resistance - due to the changing state of the high-side switch, and a varying low-side resistance - due to the changing state of the low-side switch. This leads to four possible configurations, of which every configuration also has a range of possible capacitor voltages.

- High side switch and low side switch do not conduct
- High side switch conducts, low side switch does not.
- High side switch does not conduct, low side switch does conduct.
- Both low side and high side switch are conducting.

In each case the voltage across the NEA is compared with the circuit's supply voltage and converted to a logical high or low signal. In order to accurately differentiate whether the NEA has been deployed or not, a 1 Ohm series resistance was added. In order to allow for a difference in voltage across the NEA even when the capacitor is not charged, the 28V line from the lander is connected to the circuits supply node through a resistor. Furthermore, a resistor is added in series from the NEA to ground. These two resistors connected from 28V through the circuit to ground allow a small amount of current to flow, enabling effective voltage measurements independent of the capacitors' state of charge and the conduction mode of the high and low side switches. This is possible as the NEAs have a rated no-fire current, beneath which they are guaranteed not to deploy. This configuration leads to the circuit as shown in the Figure 6.7.

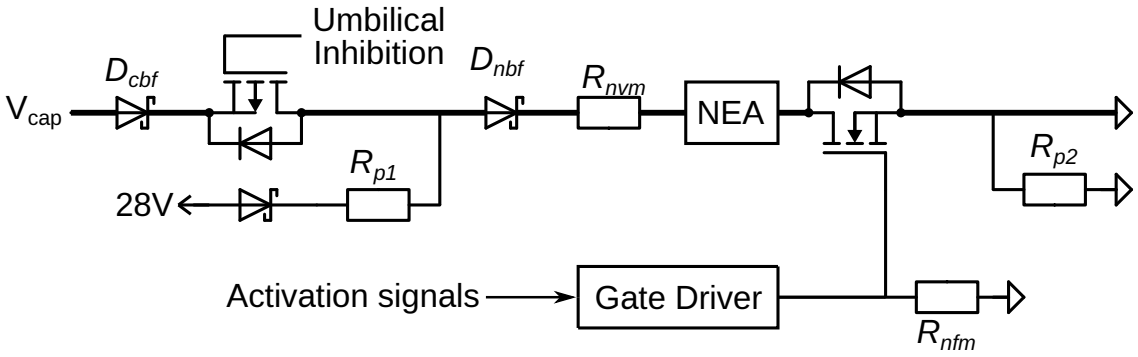

Figure 6.7: The NEA actuation circuit without sensing amplifiers

Because the NEA behaves like a fuse, the connection becomes an open circuit when the NEA is deployed. This leads to the cases in Tables 6.4, 6.5, 6.6, and 6.7, assuming node A,B and C as specified in Figure 6.8. The calculated voltages assume that the on-resistance of the MOSFETs is negligible, whereas their cutoff resistance is infinite. Each time, the upper table shows the situation when the capacitor is completely discharged, whereas the lower table shows the values when the capacitor is fully charged.

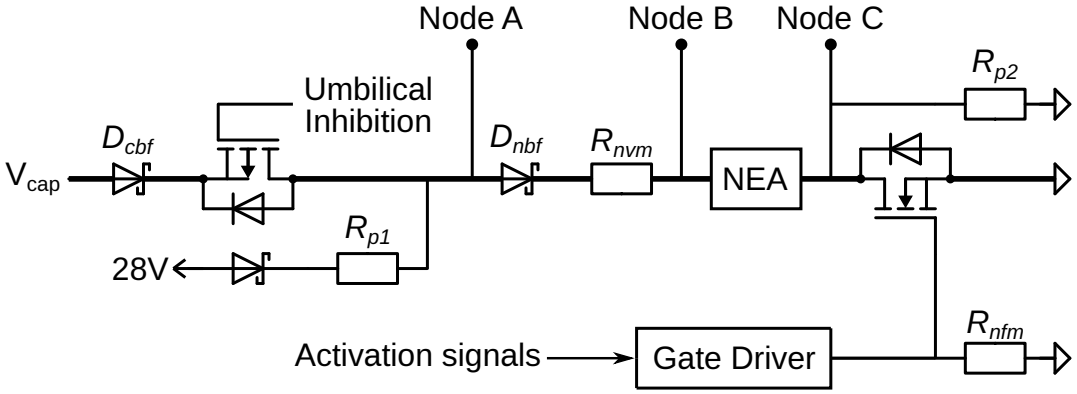

Figure 6.8: Specification of Node A, B and C

Table 6.4: High, low side switch do not conduct. Vcap=0V, 28V.

	Undeployed	Deployed
Va	21.6	28.00
Vb	20.96	28.00
Vc	20.96	0.00

	Undeployed	Deployed
Va	21.60	28.00
Vb	20.96	28.00
Vc	20.96	0.00

Table 6.5: Only high side switch conducts. Vcap=0V, 28V.

	Undeployed	Deployed
Va	21.6	28.00
Vb	20.96	28.00
Vc	20.96	0.00

	Undeployed	Deployed
Va	27.36	28.00
Vb	26.72	28.00
Vc	26.72	0.00

From these scenarios, it can be seen that there is no clear relation between two nodes indicating whether the NEA has deployed. Since an active low signal is preferred in order to simplify the lander override system, as specified in Section 6.3, the relation $V_b - V_c < \frac{3}{4} \cdot V_a$ was chosen, which is only ever untrue when the NEA has deployed. This relation was implemented by means of a subtracting amplifier and a comparator, as shown in the Figure 6.9. Note that the final signal is scaled down and protected with a TVS diode in order to fall within the safe detection range of the microcontroller.

The complete component values of the NEA activation system are shown in the Table 6.8.

Table 6.6: Only low side switch conducts. Vcap=0V, 28V.

	Undeployed	Deployed
Va	0.69	28.00
Vb	0.00	28.00
Vc	0.00	0.00

	Undeployed	Deployed
Va	0.69	28.00
Vb	0.00	28.00
Vc	0.00	0.00

Table 6.7: Low, High side switch conduct. Vcap=0V, 28V.

	Undeployed	Deployed
Va	0.69	28.00
Vb	0	28.00
Vc	0	0.00

	Undeployed	Deployed
Va	27.1	28.00
Vb	16.1	28.00
Vc	0	0.00

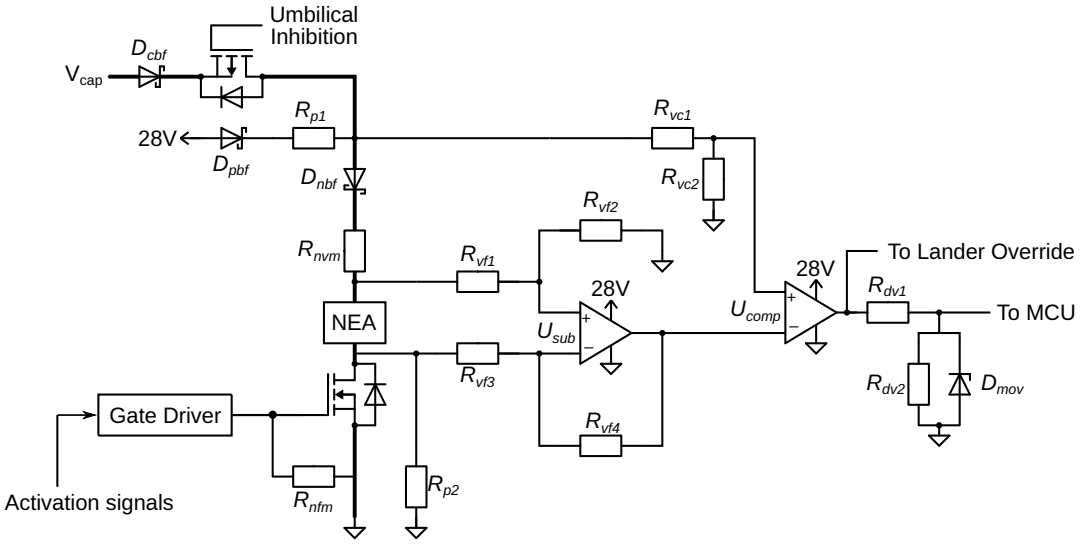

Figure 6.9: The NEA circuit and its sensing components

Reference	Value
D_{cbf}	15SQ045
D_{nbf}, D_{pbf}	SD103AWS
D_{mov}	D1213A-01T
R_{p1}	$11k\Omega$
R_{vc1}	$33k\Omega$
R_{vc2}	$100k\Omega$
R_{nvm}	1Ω
R_{vf1}, R_{vf2}	$1M\Omega$
R_{vf3}, R_{vf4}	$1M\Omega$
R_{p2}	$40k\Omega$

Reference	Value
R_{nfm}	$1M\Omega$
R_{dv1}	$120k\Omega$
R_{dv2}	$15k\Omega$
P-channel MOSFET	FQA9P25
N-channel MOSFET	IRFI4321PbF
NEA	EBAD NEA, 9040 or 1120-05
U_{comp}	TL331
U_{sub}	OPA171
Gate Driver	UCC27537DBVR

Table 6.8: Table showing component values for the NEA activation and sensing circuit

Note on Diode Placement

The circuit shows multiple diodes, such as D_{cbf}, D_{pbf} and D_{nbf}. D_{cbf} D_{pbf} are placed such that the 28V line is not affected by the change in capacitor voltage, seen as the 28V plane is used to power many components. Furthermore they ensure that the 28V signal does not charge the capacitor when it is not wanted. Since the inductance of the NEA's fuse wire is not known, it is possible that a large transient may arise when the fuse burns out. D_{nbf} is used to limit the transients effect on the rest of the circuit.

6.3. Lander Override

The authors intend to design a system that can still deploy the rover in case the MCU no longer operates. For designing such a system, a control system is still needed. The lander override system that was designed, assuming that it is possible for the lander to pull 2 lines to 28V, which would normally be at 0V.

6.3.1. Multiplexing

Because every gram counts, the capacitor bank might be sized such that it is not possible for all the NEAs to be deployed during one capacitor discharge cycle. Thus arises a need for multiplexing. This can be done in a space-multiplexing fashion, where each NEA would have its own capacitor bank. This is makes little sense when taking the requirementsof low weight into consideration, so the authors chose to work with time multiplexing.

6.3.2. Override Design

Schmitt Trigger

The first important factor to work with is the charging of the capacitor. Discharging should only occur once the capacitor has acquired enough charge to deploy a NEA. The capacitor bank should then discharge until the current is no longer high enough to deploy the NEA. A Schmitt trigger was used to achieve this behaviour, which is shown in Figure 6.10.

The operational amplifier in the design is placed in comparator figuration. The design of the Schmitt trigger has the following effect: the output voltage of the comparator will be near the positive rail ($V_{posrail}$), until the voltage at the negative terminal crosses a certain threshold ($V_{thres,pos}$). Once this voltage at the negative terminal is high enough, the output will swing closer to the 0V rail ($V_{negrail}$). The comparator will continue outputting near 0V until the voltage at the negative terminal crosses a lower negative threshold ($V_{thres,neg}$).

The threshold values are set by sizing the resistors relative to each other. Assuming the comparator outputs close to its supply rails, and its lower rail is GND, the design equation for these resistors is as given in Equations 6.3 up to 6.6.

$$\alpha = V_{posrail}/V_{thres,pos} - 1 \tag{6.3}$$

$$\beta = V_{posrail}/V_{thres,neg} - 1 \tag{6.4}$$

$$R_{st3} = R_{st1} \cdot \frac{\alpha + \alpha\beta}{\beta - \alpha} \tag{6.5}$$

$$R_{st2} = \frac{R_{st3} \cdot R_{st1}}{R_{st3} + R_{st1}} \cdot \beta \tag{6.6}$$

$$\tag{6.7}$$

Signal Routing

The time multiplexing as described in Section 6.3.1 is implemented using 4 transistors. This is depicted in Figure 6.10. The NEA_activated signals are active-low signals, while the ActivateNEA signals are active-high. In this way the NEAs fire in order, and the capacitor will stop discharging once it no longer has enough charge to activate a NEA. It will then start charging again, repeating until all NEAs are deployed.

The components associated with this system are shown in the Table 6.9.

Interaction with Other Systems

Systems such as the umbilical inhibitor and override described in Sections 6.1.4 and 6.1.5, are normally dependent on MCU control signals and other signals before they allow deployment of the NEAs. These systems have been adapted so as to allow NEA deployment if the second override signal from the lander is also pulled high. One example of this is the capacitor charge flag, where the capacitor is able to charge.

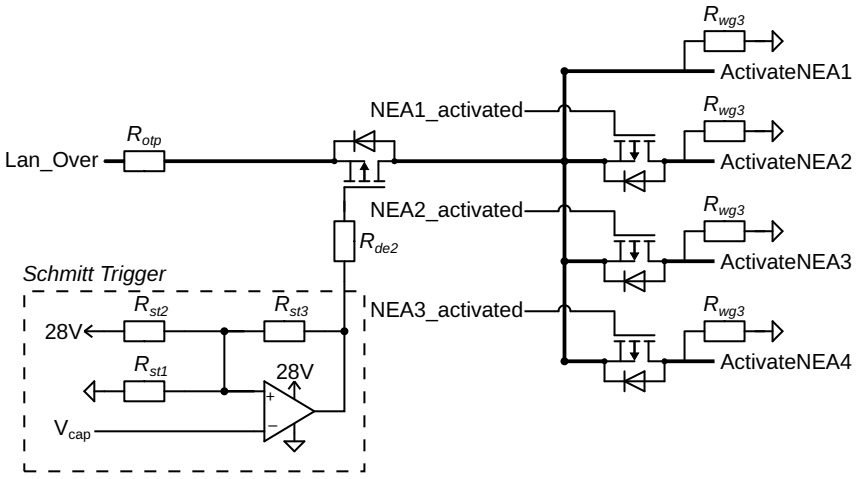

Figure 6.10: Schematic of Lander Override System

Reference	Value
R_{otp}	$1k\Omega$
R_{st1}	$140k\Omega$
R_{st2}	$56k\Omega$
R_{st3}	$40k\Omega$
R_{de2}	$47k\Omega$
R_{wg3}	$1M\Omega$
P-channel MOSFETS	DMP510DL-7
Comparator	TL331

Table 6.9: Component references and values for the lander override system

Requirements

This system conflicts with requirement 2 of Section 3.1.1, as it is unknown if the rover battery is charged at the time of deployment. However, if communication is lost between the MCU and the lander, this system could save the mission. Thus, this system is used as a backup system.

6.4. Thermal Sensing

One part of the challenge of extraterrestrial missions lies in the management of extreme swings in temperature. In these conditions, especially near the lower end of the temperature range, not all electronics are guaranteed to work, so it is essential for the RDS to be able to measure its temperature and heat itself. This section will explain the design of the temperature sensors that send their signal to the MCU.

6.4.1. Measuring temperature

There are multiple types of electrical components that are commonly used to measure temperature. For this design, the authors chose to use a Positive Thermal Coefficient resistor (PTC). This was done as resistors are relatively cheap, simple, and easy to read out, and PTC resistors have a more linear response to temperature variations than other options. PTCs are also long-term stable, meaning they experience little drift over time [20].

For reading out the temperature from the PTC resistor, a Temperature Dependent Oscillator topology was used based on a 555 timer. These designs have been shown to work well in extreme temperature, and to experience almost no deviance in frequency from the extreme temperatures [21].

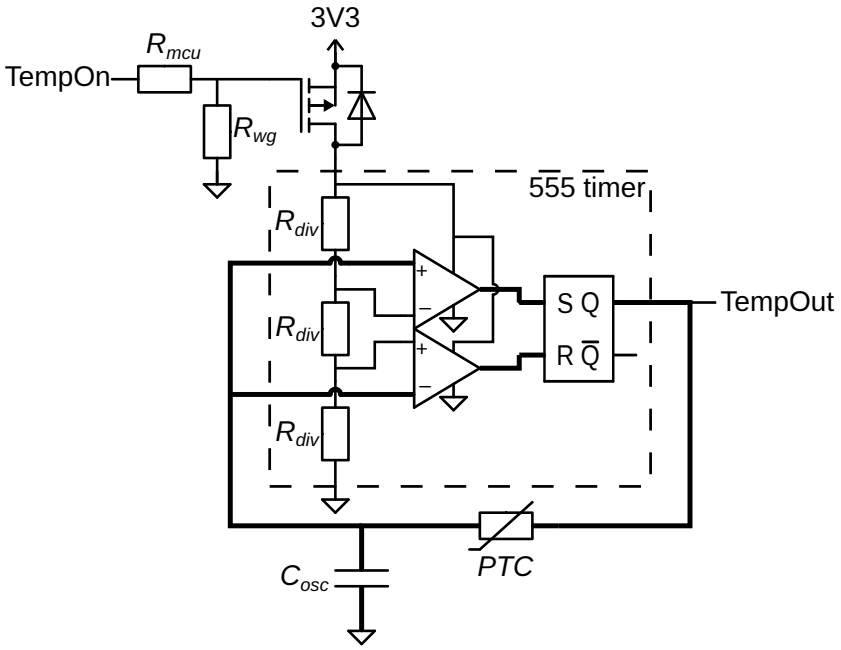

Figure 6.11: Schematic of Temperature Dependent Oscillator

Reference	Value
R_{mcu}	$1k\Omega$
R_{wg}	$47k\Omega$
P-channel MOSFET	DMG1013T
C_{osc}	$2.2\mu F$
PTC	P1K0.232.6W.A.010
555 Timer	LMC555CMX

Table 6.10: Components chosen for the Temperature Dependent Oscillator

6.4.2. Mechanics of Temperature Dependant Oscillator

When the system starts up, the capacitor is fully drained. This means the bottom comparator will swing to a positive voltage, which in turn pulls the set input of the flip-flop high. The top comparator keeps outputting low, thus the reset input of the flip-flop will stay low. In this combination, the output (Q) is high. As Q is connected to the comparator inputs via a resistor, the capacitor at the inputs will start charging.

The capacitor will continue charging until the reset input of the flip-flop is pulled high. This happens when the capacitor voltage is two-thirds of Vcc. When this occurs, the reset input will be pulled high, and the set input will be low. Q will then be pulled low, and the capacitor will start discharging via the resistor into Q. The capacitor will continue discharging until the capacitor voltage is equal to one third of Vcc, when the set input of the flip-flop is pulled high once again.

This is the same state as in the first paragraph, and the system thus enters a loop, where the frequency is dependant on the time constant, τ, which is the resistance multiplied by the capacitance.

If the resistor between the flip-flop output and the comparator inputs is a temperature dependant resistor, the frequency of the system is then also temperature dependant.

Frequency as a function of temperature

$$V_{cap} = V_{cc} \cdot (1 - e^{-t/RC}) + V_{initial} \tag{6.8}$$
$$V_{cc} = V_{cc} \cdot (1 - e^{-t/RC}) + 1/3 \cdot V_{cc} \tag{6.9}$$
$$Solve for e^{-t/RC} = 1/2 \tag{6.10}$$
$$-t/RC = ln(1/2) \tag{6.11}$$
$$t_{charge} = 0.69 \cdot R \cdot C \tag{6.12}$$
$$t_{discharge} = t_{charge} \tag{6.13}$$
$$f_{timer} = \frac{1}{t_{discharge} + t_{charge}} = \frac{1}{2 \cdot t_{charge}} \tag{6.14}$$
$$f_{timer} = \frac{1}{2 \cdot 0.69 \cdot RC} \tag{6.15}$$
$$\tag{6.16}$$

6.4.3. Component values

A PTC was chose with a resistance of 1000 Ohms at $0°C$. This resistance value was chosen as it was one of the higher values available on the market. This is advantageous both in terms of power draw, and the absolute resistance changing more per degree temperature increase.

The frequency is a function of the capacitance and resistance. As the MCU team preferred a frequency range between 100 and 900 Hz at the time of design, a capacitance of 2.2 μF was chosen. This corresponds to a frequency range of 415-250 Hz inside the temperature range of -55 up to 80 degrees Celsius.

6.5. Backup temperature sensor

The temperature dependant oscillator described in Section 6.4 is only useful if the microcontroller can turn a heating system on or off. Else, failure in this component could lead to the entire RDS overheating. If the temperature drops below -55° - which is the lowest temperature for which the microcontroller is rated [22] - the heating should still be turned on. This entire system should work on the 28V rail, as it might be needed to heat the buck converters which supply 3.3V to the microcontroller.

Mechanics of the backup temperature sensor

The backup temperature sensor should turn off above a certain temperature, as to prevent overheating. However, it is important for the backup temperature sensor to have an element of hysteresis, as it might start jittering at the threshold temperature. To achieve this, another Schmitt trigger was used, similar to Section 6.3.2. At the negative terminal, a resistive divider to GND was used, incorporating the PTC described in Section 6.4.3. This design can be seen Figure 6.12.

6.5.1. Heater Resistor

Heating is implemented by means of a power resistor with a large thermal pad and a strong connection to the ground plane, placed close to the buck converters and the microcontroller, which have been designated as the most critical temperature dependent devices of the system. Whether or not power flows through this resistor is decided by a system of two low-side switches. One of these switches is directly driven by the microcontroller, in order to allow power to flow through the resistor. The other switch is driven by the backup thermal sensor, but can be overridden by the MCU to turn the system off. The gate of both switches is connected to ground through a large resistor, indicating that the standard mode of the system is ”off”. The microcontroller can read the status of the resistor, through the same resistive divider and TVS diode combination as described in Section 6.1.3. The complete system is shown in Figure 6.12, in which R_h indicates the heating resistor.

The components chosen for this system are shown in Table 6.11.

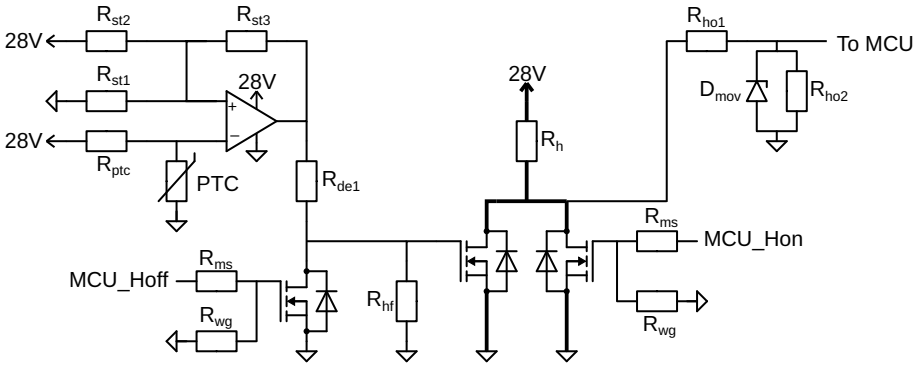

Figure 6.12: Design of Heating System and Backup Temperature Sensor

Reference	Value
R_{st1}	$1k\Omega$
R_{st2}	$190k\Omega$
R_{st3}	$2.5M\Omega$
R_{ptc}	$200k\Omega$
R_{de1}	$200k\Omega$
R_{ms}	$1k\Omega$
R_{wg}	$47k\Omega$
R_{hf}	$2M\Omega$
R_h	800Ω
R_{ho1}	$120k\Omega$
R_{ho2}	$15k\Omega$
PTC	P1K0.232.6W.A.010
Comparator	TL331
N-channel MOSFET	SI2306

Table 6.11: Components chosen for the heating system and backup temperature sensor

6.6. Current Sensing

In order to monitor the charging of the rover's battery, a current sensor is used. This sensor is implemented by the use of a shunt resistor, connected to a voltage amplifier with a set gain. The authors have selected Texas Instrument's INA2504A to fulfill this purpose. This component uses a $2m\Omega$ shunt resistor and has an equivalent gain of $2V/A$. Considering the current through the shunt resistor will likely not be more than $\frac{1}{4}A$, this gain offers the highest resolution when connected to the microcontroller out of the INA250 series, while still offering a large amount of headroom in case of higher currents.

6.7. PCB Design

Traces on a PCB have inherent resistances, capacitances and inductances. Therefore, it is usually better to place components close to each other, such that they do not require long traces in order to connect to each other. In the case that this is not possible, dwindling and circular paths are best avoided, in order to minimise parasitic inductance and capacitance. Furthermore, longer traces can be thickened in order to reduce their resistance. However, this causes the trace to have a larger surface area, causing them to be more susceptible to interference and coupling with other traces. In cases where added resistance to the path is problematic, such as in the case of large currents, a trace width calculator can be used to estimate the resistance of a path, or calculate the probable width to stay below an acceptable limit. In the case of the path from the capacitors to the NEAs, a width calculator was used to ensure that the equivalent resistance did not exceed 0.5Ω

Test pads are placed in as many places as is realistic, such that the verification of proper functioning of the systems, as well as any debugging, is made easy. These test pads are placed for any relevant

signals and voltages and should always have a ground pad nearby.

Most resistor and capacitors are chosen to have a 0805 (2012 metric) SMD footprint. This allows them to be soldered by hand with relative ease, but also allows the PCB to be assembled by means of a pick and place machine. Considering the PCB has more than 300 components on board, assembling it by hand is a tedious and time consuming endeavour.

All resistors are chosen to have at most 1% tolerance and at most 100ppm/K temperature variability. When the continuous power dissipated by the resistor falls below 1/16W, a 1/8W rated resistor was chosen. Otherwise, the power rating was chosen as double the continuous power, rounded up to the nearest half Ohm.

The components surrounding the microcontroller usually feature 0402 or 0603 footprints, as there is very limited space around the microcontroller on the PCB because of the large density of traces connecting the MCU to all other systems.

7

Testing Methodology

7.1. Simulation Testing

Before ordering parts and commencing physical testing, it is essential to simulate designs first. In this way, issues can come up before parts are bought, saving both time and money.

All designs should be simulated in LTSpice. For a situation where control signals are used, all possible combinations of input signals must be tested.

7.1.1. NEA Simulation Model

In order to model the NEA for use in simulations, an equivalent model was designed, consisting of a current sensing voltage source, an equivalent resistance, a voltage dependent switch and three conditional voltage sources. The model makes use of I2T modeling, meaning that it requires a combination of current and time to burn out the fuse. The model behavior is adjusted by setting the $I2T_{max}$ parameter as well as $Imin_{melt}$, which is the minimum current required to start burning out the fuse. This model is shown in Figure 7.1.

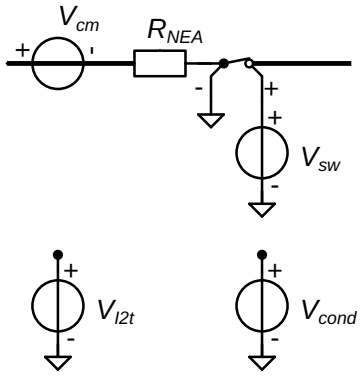

Figure 7.1: Fuse simulation model

The model functions by integrating the square of the current through the NEA with respect to time. If this integrated value exceeds $I2T_{max}$, the switch to the NEA is opened, creating an open circuit. The first dependent voltage source in the model is only active if the current through the current sensing source exceeds $Imin_{melt}$. This dependent source then generates a voltage equal to the current through the current sensor. The second dependent voltage source integrates the square of the first dependent voltage source with respect to time, creating the model's $I2T$. The last dependent voltage source opens the voltage controlled switch if $I2T$ exceeds $I2T_{max}$, indicating that the fuse has burned up and no current can flow through the model. LTSpice does not offer a simple method of setting bounds to the integration, meaning that the fuse model cannot be reset in case of partial activation.

7.2. Physical Testing

In order to verify whether the requirements are truly met, the system requires rigorous physical testing.

The authors intend to test the NEA deployment circuitry for at least 25 complete deployment sequences of 4 fuses at room temperature. Furthermore, it will be put through cycles of cooling to -120° C and back to ambient and then tested at -60° C either until failure or up to 10 times. Similarly, the system will be heated up and deployed at 120 ° C until failure, or up to 10 times. Every single one of these tests should be succesful: any failure should prompt an investigation into their cause.

The lander override and umbilical override backup systems must be tested completely separately. A failure in a main system test should not be classified as a success by means of a backup system. The main system should work 100% of time and the backup system should work 100% of time.

The Thermal management system should be checked at many possible temperatures, where both the activation of the heating system and the frequency output of the temperature sensor must be verified Temperature sensor check frequencies at all temperatures. This data is also incredibly valuable for the calibration of the temperature sensor.

The complete system should be checked during a vacuum test, preferably undergoing multiple cycles. During vacuum tests, both the immediate functioning of the system and its long term stability should be evaluated. The system's thermal equilibrium point and its implications should be evaluated.

Testing in high acceleration environments is necessary in order to assess the system's ability to satisfy its acceleration requirement. However, it is unlikely that a proper analysis of the effects of acceleration can be done by the authors, considering their lack of expertise on mechanical systems.

7.3. Evaluation of physical test results

The RDS plays such a significant role in achieving a success for this mission that any unsuccessful tests are reason to cause alarm. Preferably, there would be no unsuccessful tests at all. After executing a statistically significant number of experiments, a confidence interval could be taken to estimate the chance of failure. Whether or not the requirement is met could be decided based on this confidence interval. It could be decided that this interval is only valid if all failed experiments involved circumstances that are beyond the requirements. All failure cases within the circumstances specified by the requirements could immediately indicate the requirement is not met.

8

Results

For all simulation results, the schematics which were used to simulate can be found in Appendix C.

8.1. NEA Sensing and Actuation

The sensing and actuation system draws 2.36mA in simulation, corresponding to 66mW. The simulations once again make use of three nodes: A, B, and C, as shown in Figure 8.1.

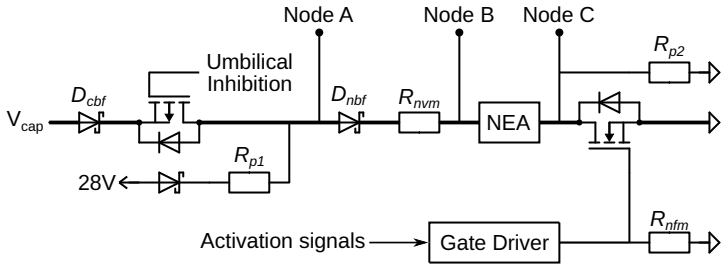

Figure 8.1: Specification of Node A, B and C, copy of Figure 6.8

8.1.1. NEA Deployment Sensing

Figure 8.2 shows a situation wherein the capacitor is used to deploy multiple NEAs. The capacitor voltage (node A) is shown above, followed by the voltages at node B, and C. The lower graph of the figure shows the the subtracted signal of B and C, the check signal $\frac{3}{4}V_a$ and the subsequent NEA Deployed signal. In this Figure, the deployment of the first NEA commences just after 63.40s. The deployment of the first NEA is completed just after 63.42s, after which the NEA Deployed signal immediately switches to 0V. The capacitor continues the sequence by discharging into the other NEAs. This does not change the readout of the NEA Deployed signal, which continues to operate independently of the deployment stage.

8.1.2. Expanded NEA model

When the NEA was simulated as a fuse, a resistance, and a 1uH self-inductance, no difference was found in the results of the simulation.

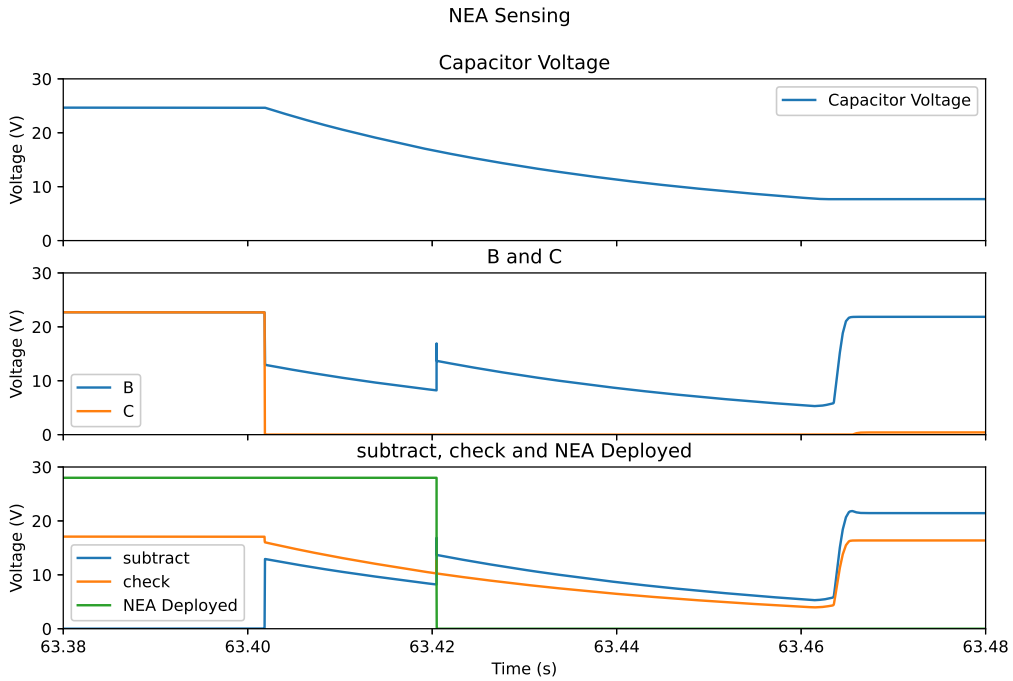

Figure 8.2: NEA Deployment Sensing. Nodes B and C are as in 8.1

8.2. Umbilical Inhibition and Activation

As can be seen in Figure 8.3, the NEA will not deploy if the PMOS gate signal is high. As the umbilical cord is connected to the gate of the PMOS via internal logic (Section 6.1.4), the NEA will not deploy while the umbilical cord is connected. Similarly, deployment does not commence if only the activation signal is sent. The deployment only commences when both the inhibition system and activation system are driven into conducting state. In simulation, this system draws 0W.

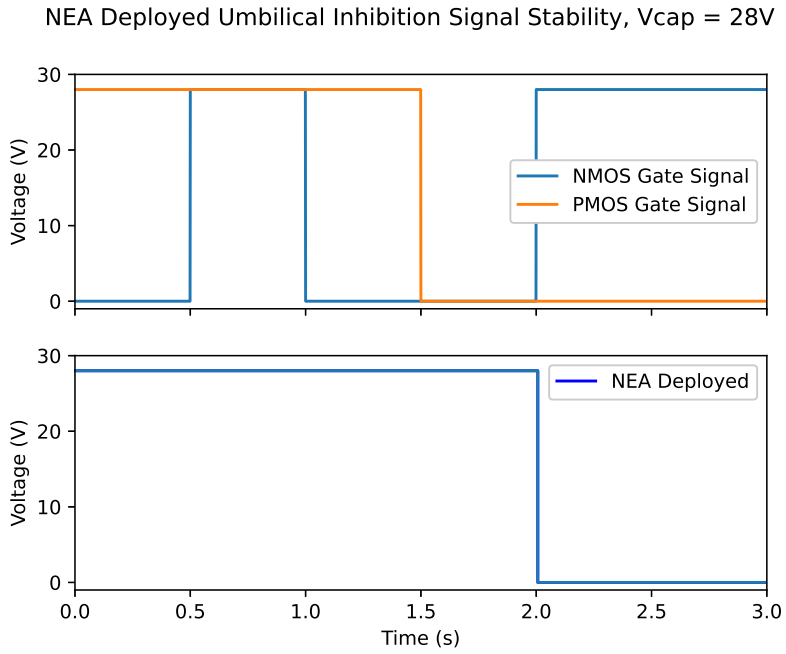

Figure 8.3: Simulation of Umbilical Inhibition

Figure 8.4 shows that the readout of the NEA Deployed signal does not change based on the status of the activation and inhibition systems, as long as the NEA is deployed. Figure 8.5 shows that the activation and inhibition systems do not change the readout when the NEA is undeployed. Thus, whether the NEA Deployed signal is high or low is solely dependent on whether the NEA is deployed and is not affected by the operating mode of the actuation circuit.

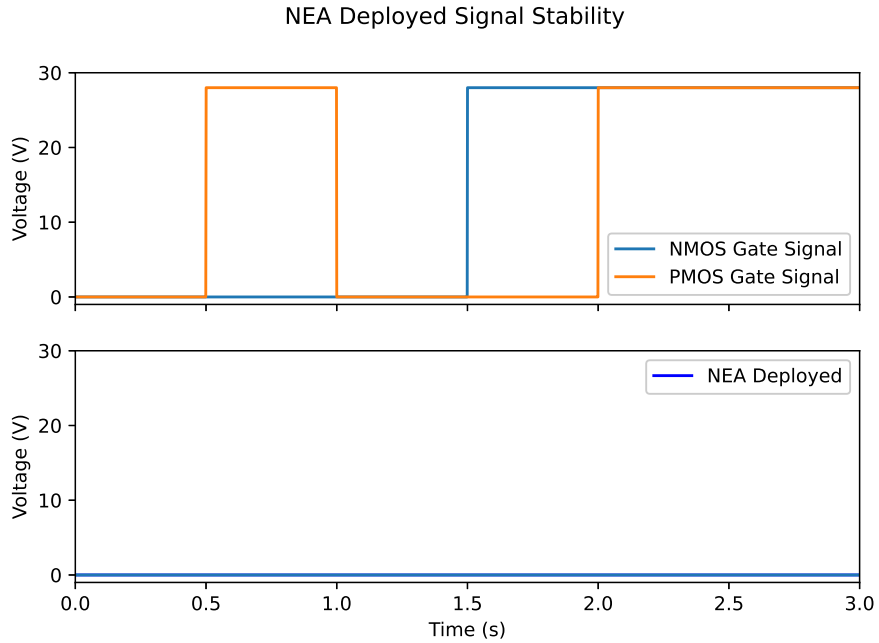

Figure 8.4: NEA Signal stability when NEA has been deployed

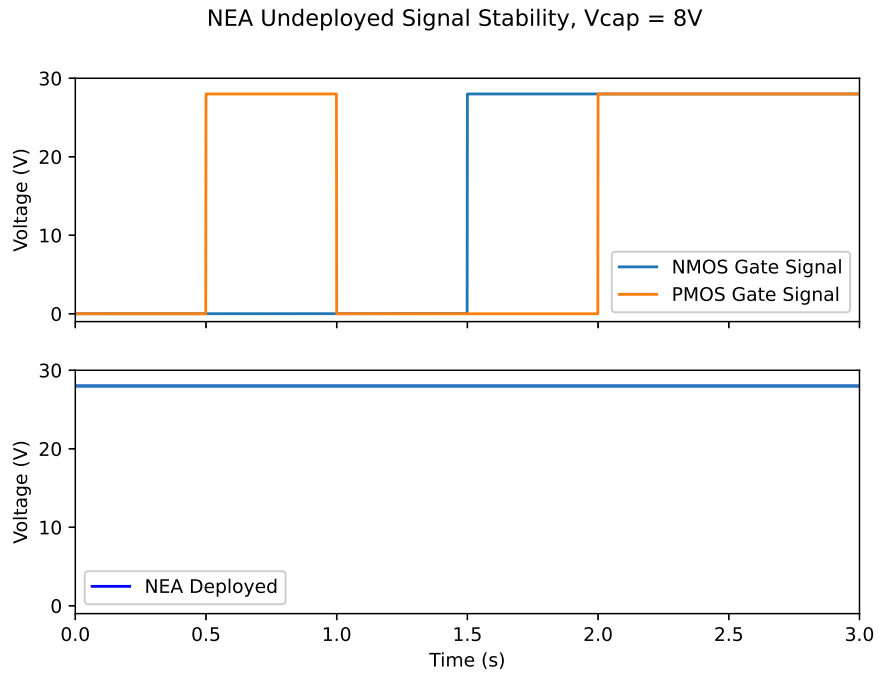

Figure 8.5: NEA Signal stability when NEA has not been deployed and the capacitor does not have enough charge to deploy the NEA

Figure 8.6 shows the possible cases for the input logic of the inhibition p-channel MOSFET. The MOSFET is conducting when the umbilical cord is not connected and when both the rover and MCU override are high.

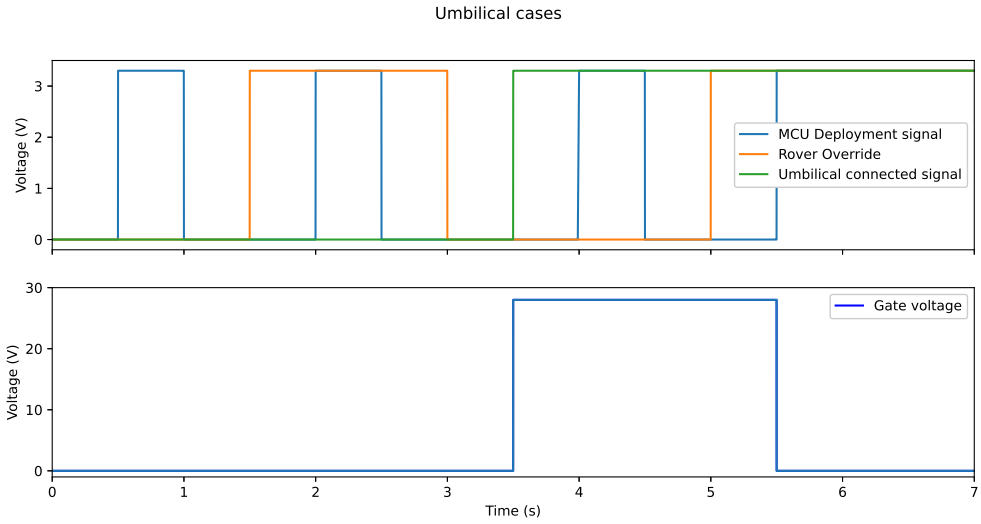

Figure 8.6: PMOS gate voltage vs control signals

8.3. Lander Override

As the lander override system needs a working NEA activation and sensing system, a simulation was done with the above-mentioned NEA simulation circuit. The result of this complete simulation can be seen in Figure 8.7. The capacitor voltage steadily rises, until deployment is possible. The first NEA deploys, at which point the capacitor is drained. Therefore, the capacitor starts charging again to discharge the next NEA. This cycle repeats until all NEAs have been deployed.

When deploying the last NEA, the capacitor voltage only dips slightly before deployment is complete. This is due to the known shortcoming mentioned in Section 7.1.1, where a fuse can partially burn through. However, this will not be a problem in physical testing, as the capacitor will always be able to deploy a NEA in one discharge cycle[1].

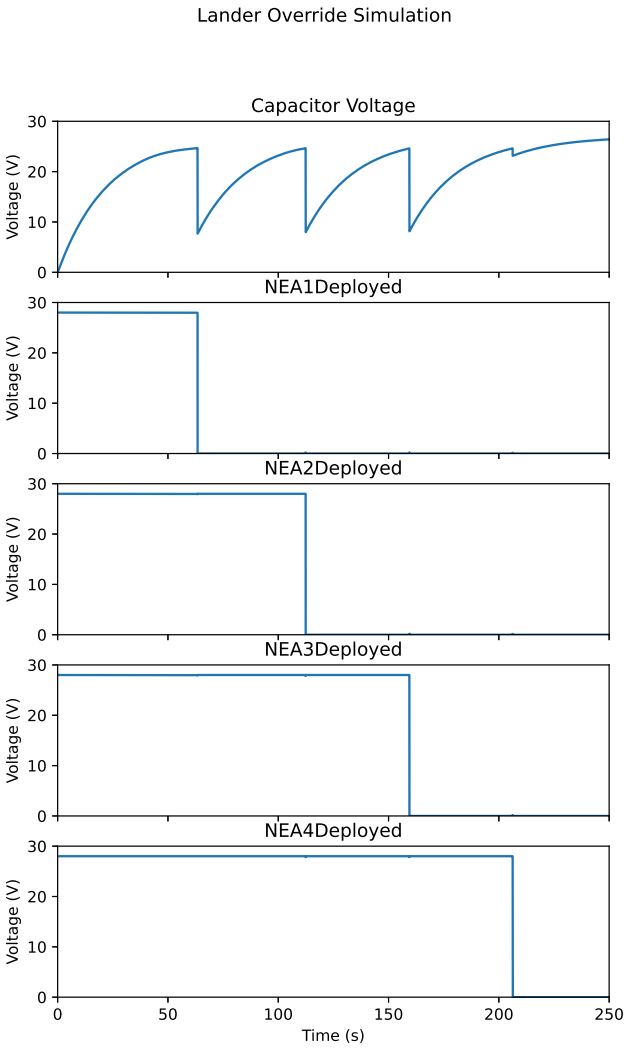

Figure 8.7: Simulation of Lander Override System

[1]This specific capacitor sizing is done by the power system team [8]

8.4. Temperature Sensing

For the temperature sensor using a 555 timer, as described in Section 6.4, a python script was written to calculate the expected temperature for a given frequency. This relation can be seen in Figure 8.8. The code used to generate this figure can be found in Section B.1 in the appendices.

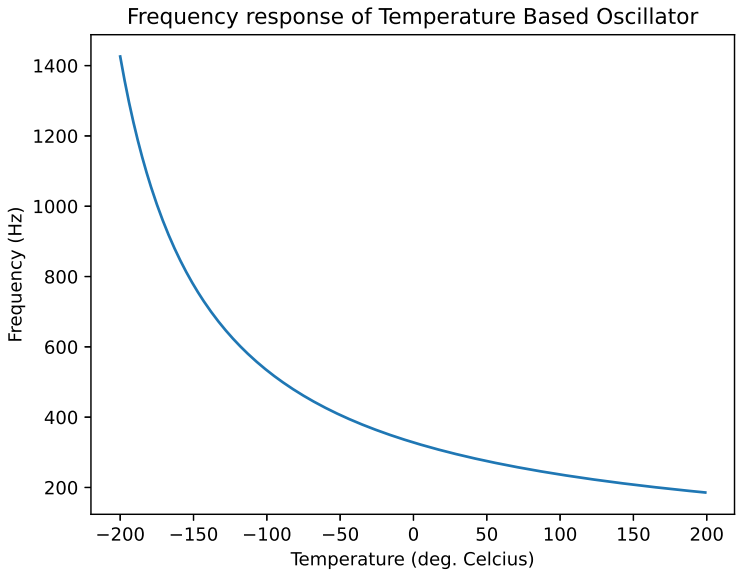

Figure 8.8: Calculated Frequency for a given Temperature

The simulation results of a single temperature sensor can be seen in Figure 8.9. The capacitor charges and discharges as expected, and this lines up with the comparator output. The frequency also matches: the simulation was done with a 1k Ohm resistor, matching expectations.

The temperature sensors draw approximately 1.5mA per sensor in simulation, corresponding to a total power draw of 10mW. However, this simulation was done with a generic 555 timer, and it is thus uncertain if this power draw is a realistic figure.

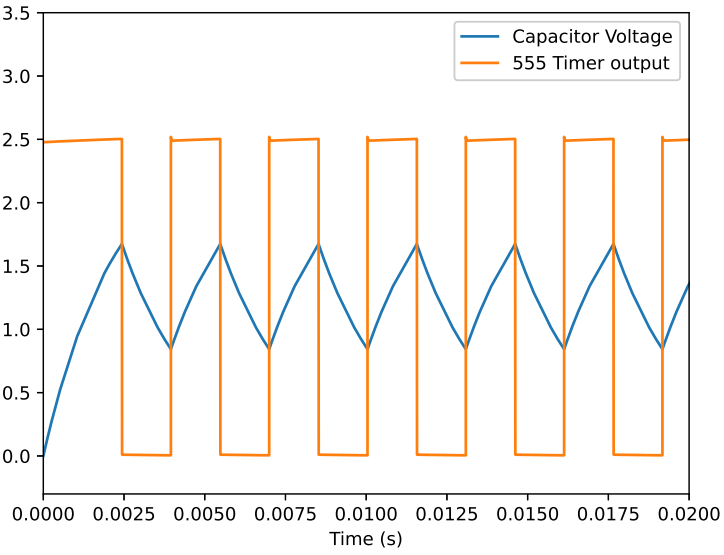

Figure 8.9: 555 Timer-based Temperature Sensor

8.5. Backup Temperature Sensing and Heating

Figure 8.10 shows the possible combinations of MCU input signals and the corresponding heating status. The top figure shows the input of the schmitt trigger used for backup temperature sensing. This is a sine wave that oscillates between voltages that correspond to reasonable temperatures. If the MCU sends no control signals, the heating follows the backup temperature sensor. If the MCU does send control signals, these control signals set the heating status.

The system draws 35mA when actively heating, and draws 0.43mA when not heating. This corresponds to 1W and 12mW respectively.

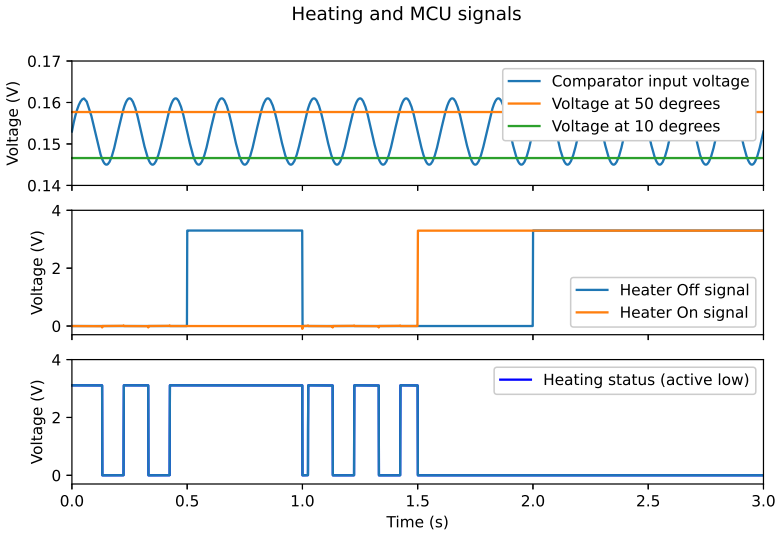

Figure 8.10: MCU control signals and corresponding Heating status

8.6. PCB Design

At the time of the publication of this report, the PCB corresponding to the integrated electronic test design is completely routed and ordered, however not delivered. Therefore it has not been possible to execute tests of physical systems. An image of the front and backside of the routed PCB can be seen in Figure 8.11. The PCB and its components are sized 196mm by 178mm with a height of <70mm. A PCB of this size usually weighs between 150 and 250grams excluding any components.

The PCB contains test pads for measuring the three most relevant voltages on the board, namely 3.3V, 12V and 28V. Furthermore there are many ground pads that enable more accurate voltage measurement at many points of the PCB. All inputs and outputs of the microcontroller, as well as the outputs of the lander override system, are linked to test pads for easy measurement. Lastly, the capacitors have separate test pads such that their voltage can be measured, which enables tuning of the microcontrollers measurement system. This tuning could be relevant as the scaling of the signal in - order to fall within a safe reading range for the microcontroller - could introduce a measurement inaccuracy.

The PCB features four fuseholders in series with NEA equivalent power resistors, such that the activation of the NEAs can be simulated. The board also contains screw terminals such that any alternative NEA simulator may be used. This would allow testing with various amounts of load inductance, capacitance and variable resistance. The NEAs itself could also be connected here, although this is unlikely due to their significant single use cost. All designators and component courtyards are printed on the backside silkscreen layer, such that component malfunctions and replacements can be easily linked to the digital design files. The backside of the PCB is shown in Figure 8.12.

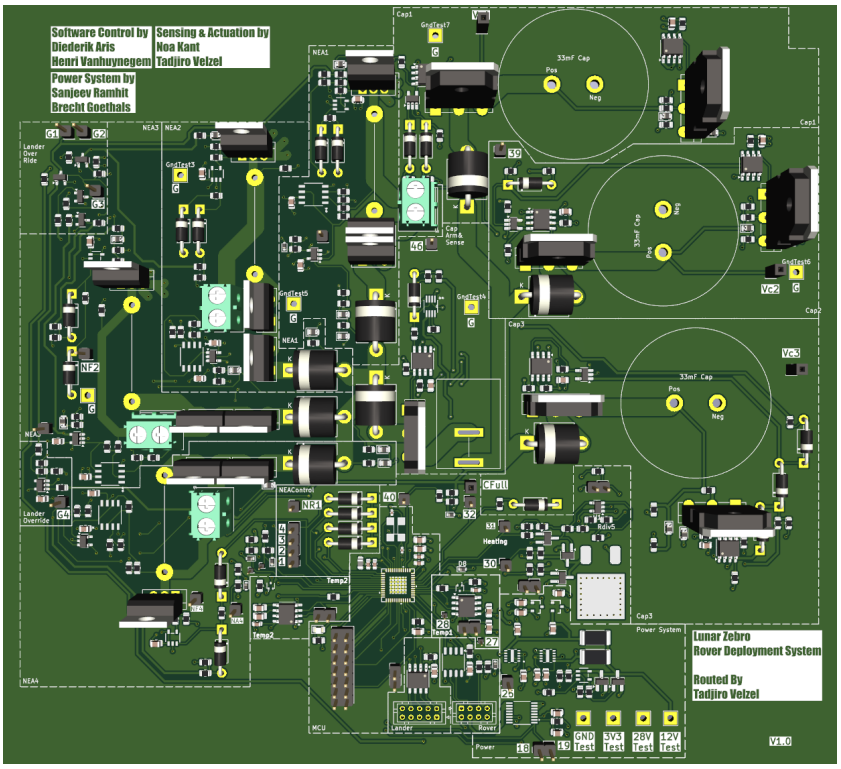

Figure 8.11: Frontside of the system PCB

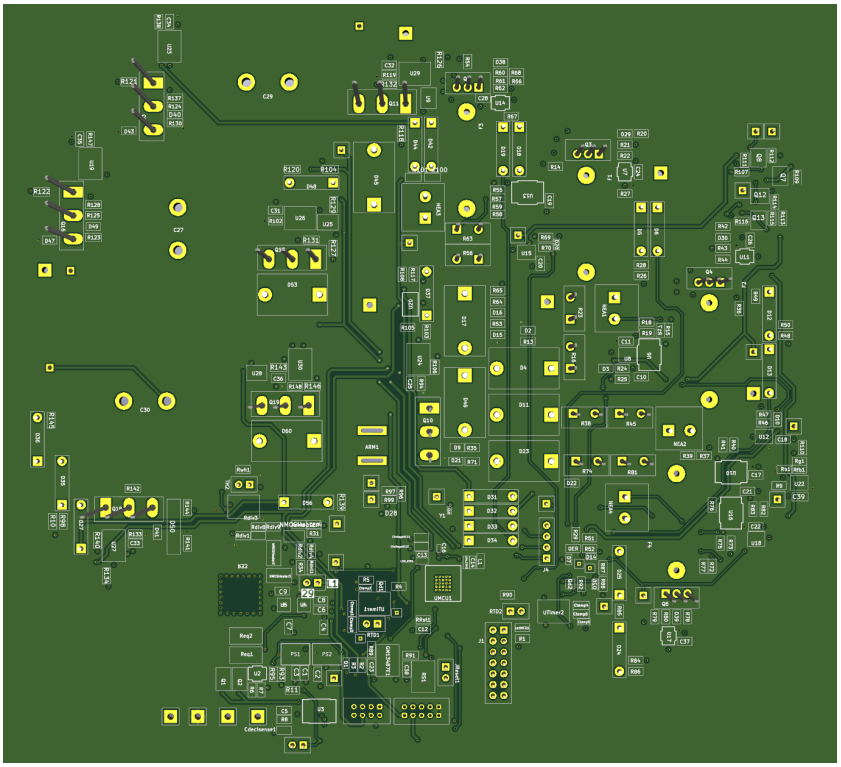

Figure 8.12: Backside of the system PCB

9 Discussion

9.1. Meeting of Requirements in Simulation

9.1.1. Functional Requirements

The authors have designed a system which is able to deploy 4 Non-Explosive Actuators by means of sequentially supplying more than 4A for 50ms to each NEA - as shown in Figure 8.7. In simulation, this process spanned 250 seconds Figure 8.7. This sequence is inhibited by a physical connection to the rover by means of an umbilical cord Figure 8.3. This cord can be overridden when the rover and microcontroller send an override signal at the same time Figure 6.4. The deployment of the NEAs is initiated by an activation signal sent by the RDS' microcontroller Figure 6.6. This initiation will only happen when the rover is ready to deploy [7]. The system contains a heating element that can be used to regulate the temperature Figure 6.11. Thermal regulation can function independently of a digital control system, but can also be managed by the microcontroller Figure 8.9. In the case that the microcontroller experiences failure, the NEA activation sequence can be initiated by two control signals from the lander Figure 8.7.

Thus, this system satisfied the functional requirements as stated in Chapter 3:

1. The system must be able to actuate 4 Non-Explosive Actuators [1]
2. The NEAs must not activate until the rover is ready for deployment
3. The system must activate the NEAs when the rover is ready for deployment
4. The system must be able to actuate the 4 NEAs within 120 minutes

9.1.2. Non-functional Requirements

Chapter 3 also specifies the following non-functional requirements:

1. An umbilical cord must be used to connect the RDS to the Rover
2. The system should be able to operate after being exposed to temperatures between -120 and +120°C
3. The system must be able to deploy the NEAs within the entire rated temperature range of the NEAs, from $-60^{\circ}C$ to $120^{\circ}C$.
4. The system should be able to withstand 6g of constant acceleration, and 9g of peak acceleration.
5. The system should be able to operate on 3W, 28V DC supply.
6. The system must be able to deploy the NEAs in a vacuum.

An analysis of available umbilical cords and their characteristics can be found in the thesis of the Power System [8]. The use of an umbilical cord has been incorporated into the NEA actuation design. Therefore the first non-functional requirement has been met.

[1] The specific type of NEA and its characteristics are specified in Section 4.1

In simulation, the system draws a base load of 88mW. When heating, the system draws 1.1W. This is less than the fifth requirement specifies, which the system thus theoretically meets.

The storage and operating temperature ratings of the chosen components are not a clear indicator of the system's ability to endure extreme temperatures. It is not possible to make a definitive claim regarding the system's ability to achieve temperature requirements, as simulation of exposure to extreme temperatures is not feasible.

The system's ability to withstand high acceleration is strongly tied to the mechanical properties of the PCB and its connections. Therefore the capability of the design to meet the fourth requirement cannot be definitively ascertained.

It is not possible to simulate the ability of a system to function in a vacuum. The design of the system does not include components with high outgassing probability, which is a favorable indication. However, the design's ability to function in a vacuum is also dependent on its capacity to dissipate excess thermal energy. Therefore no definitive claim can be made regarding the sixth non-functional requirement.

9.2. Trade-off Requirements

Chapter 3 specifies two trade-off requirements.

1. The rover deployment control system must weigh less than 200 grams
2. The rover deployment control system must be smaller than 20cmx20cmx10cm

The PCB meets the volume requirement, as its size is 19.6cm x 17.8cm x 7cm as specified in Section 8.6. Therefore, the second requirement is met.

According to a general estimator, the PCB would weigh approximately 150-250g excluding the capacitors, which weigh 130g per unit for a total of 390g. This does not meet the first requirement. However, as this is a test PCB, it is not unreasonable to assume that a final PCB could fall within the mass specification.

9.3. Physical Meeting of Requirements

The authors hope to use the PCB to test all simulations in physical context. However, due to logistical issues, the PCB and necessary components have not been delivered at the end date of this thesis. Due to the current lack of results outside of the simulator, there can be no discussion about whether requirements are met. The only definitive statement that can be made at this point is whether or not a physical implementation of the system has the potential to meet the requirement. The authors cross their fingers that all deliveries will be made in due time.

9.4. System Vulnerabilities

The design suffers from a major system vulnerability, namely the stability of the 28V supply. All systems on the board are either directly or indirectly dependent on the stability of the 28V line. If any component causes a short from 28V to ground, the entire system is at risk. Considering the large amount of components on the board, this probability is not negligible. A possible way to alleviate this problem is by splitting power planes, which each have an independent current sensor and a switch. A section of the board could then be completely disconnected from the 28V supply, protecting the integrity of the system.

The authors of this report have very little knowledge of thermal effects and design and did not focus on questions such as ”How does the design radiate out excessive heat?” or ”How are components best placed such that heat generation is balanced across the PCB?”. Therefore, no solutions have been implemented for dealing with temperature buildup, indicating that this is a potential system vulnerability.

9.5. Future Work

The authors intend to assemble the PCB and test its systems, if the parts are delivered on time. Tests will be executed as specified in Testing Methodology Chapter 7. These tests will be used to discuss whether the system has conclusively met the requirements.

Any design that is intended to be sent into space requires certification and optimisation for the space environment. Robust components and manufacturing methods need to be chosen that have an improved ability to survive the harsh conditions of space. Therefore, a redesign of the PCB that does not use vulnerable components or mechanisms for testing is necessary. Afterwards, this design can be submitted for space certification.

10

Conclusion

The authors have designed a system which is able to deploy 4 Non-Explosive Actuators by means of sequentially supplying more than 4A for 50ms to each NEA. This sequence is inhibited by a physical connection to the rover by means of an umbilical cord. This inhibition system can be overridden when the rover and microcontroller send an override signal at the same time. The thermal system contains temperature sensors and a heating element that can be used to regulate the temperature. Thermal regulation can function independently of a digital control system, but can also be managed by the microcontroller. In the case that the microcontroller experiences failure, the NEA activation sequence can be initiated by two control signals from the lander.

No definitive claims can be made about whether the system physically meets the functional requirement, as it has not been possible to conduct physical tests due to logistical issues.

This system has been verified to work in simulation. In simulation, it meets all functional requirements as specified in Chapter 3 Section 9.1. The system also meets all non-functional requirements that could feasibly be verified in simulation.

11

Conflict of Interest Statement

The assessment of this design report is critical to the academic career of the authors, as their ability to receive a bachelor's diploma is based on it. The authors declare no other relevant conflict of interest.

12

Acknowledgements

We would like to thank Chris Verhoeven, our daily supervisor, for his guidance during the project. We would also like to thank Anton Montagne, Bas Verdoes, Maarten van Schagen, and Quinten Luyten for their feedback on our designs. We would like to thank Richard Patterson at NASA for his research into components in extreme conditions. Lastly, we extend our appreciation to Roni Velzel for his extended support throughout the design process.

References

[1] Lunar Zebro | TU Delft, *Lunar Zebro website*, [Accessed 12-05-2024]. [Online]. Available: https://zebro.space/.

[2] World Economic Forum, *Space: The $1.8 trillion opportunity for global economic growth*, Accessed: 2024-06-13, 2023. [Online]. Available: https://www.weforum.org/publications/space-the-1-8-trillion-opportunity-for-global-economic-growth/.

[3] NASA, *What Are SmallSats and CubeSats?* Accessed: 2024-06-13, 2024. [Online]. Available: https://www.nasa.gov/what-are-smallsats-and-cubesats/.

[4] ISISpace, *ISIPOD CubeSat Deployer*, Accessed: 2024-06-13, 2024. [Online]. Available: https://www.isispace.nl/product/isipod-cubesat-deployer/.

[5] D. Ewick, B. Child, and G. Kaczynski, "Development of non-pyrotechnic hold down and release mechanisms for the james webb space telescope," Ensign-Bickford Aerospace & Defense Company (EBAD), Tech. Rep., 2023.

[6] R. B. Malla and K. M. Brown, "Determination of temperature variation on lunar surface and subsurface for habitat analysis and design," *Acta Astronautica*, vol. 107, pp. 196–207, 2015, ISSN: 0094-5765. DOI: https://doi.org/10.1016/j.actaastro.2014.10.038. [Online]. Available: https://www.sciencedirect.com/science/article/pii/S0094576514004160.

[7] D. Y. Aris and H. Vanhuyneghem, "Rover Deployment Software System," TU Delft, Tech. Rep., 2024.

[8] S. J. H. Ramhit and B. Goethals, "Power System: Lunar Zebro Rover Deployment System," TU Delft, Tech. Rep., 2024.

[9] Ensign-Bickford Aerospace & Defense Company, *Nea® model 1120-05 pin puller*, [Accessed 05-06-2024], 2022. [Online]. Available: https://www.ebad.com/wp-content/uploads/2022/08/NEA-Pin-Puller-Model-1120-05-released-10-28-22.pdf.

[10] Ensign-Bickford Aerospace & Defense Company, *Nea® model 9040 miniature hold down & release mechanism (hdrm)*, [Accessed 05-05-2024], 2022. [Online]. Available: https://www.ebad.com/wp-content/uploads/2021/03/NEA_Hold_Down_Release_Mechanism__HDRM__-_Model_9040_released_4-20-22.pdf.

[11] Ben, *NEA® Hold Down & Release Mechanisms (HDRM) - Ensign-Bickford Aerospace & Defense*, Retrieved: 19-06-24, Apr. 2024. [Online]. Available: https://www.ebad.com/nea-hold-down-release-mechanisms-hdrm/.

[12] R. Patterson, A. Hammoud, and S. Gerber, "Performance of various types of resistors at low temperatures," *NASA Glenn Res. Center, Cleveland, OH, USA, GESS Rep. NAS3-00142*, 2001.

[13] N. Doumit, B. Danoumbé, S. Capraro, J.-P. Chatelon, M.-F. Blanc-Mignon, and J.-J. Rousseau, "Temperature impact on inductance and resistance values of a coreless inductor (cu/al2o3)," *Microelectronics Reliability*, vol. 72, pp. 30–33, 2017, ISSN: 0026-2714. DOI: https://doi.org/10.1016/j.microrel.2017.03.037. [Online]. Available: https://www.sciencedirect.com/science/article/pii/S0026271417300884.

[14] A. Hammoud and E. Overton, "Low temperature characterization of ceramic and film power capacitors," in *Proceedings of Conference on Electrical Insulation and Dielectric Phenomena-CEIDP'96*, IEEE, vol. 2, 1996, pp. 701–704.

[15] D. D. Liu, "Reliability and other space-related characterizations of polymer aluminum capacitors," *CARTS International, Mar*, pp. 26–29, 2012.

[16] D. A. Neamen, *Semiconductor physics and devices: Basic principles. 2003*, 4th edition, 2012.

[17] R. Ibrahim, A. El-Azeem, S. El-Ghanam, F. Soliman, *et al.*, “Temperature effects on the electrical characteristics of bjts and mosfets,” *Journal of Scientific Research in Science*, vol. 36, no. 1, pp. 100–112, 2019.

[18] B. Kaczer, R. Degraeve, P. Roussel, and G. Groeseneken, “Gate oxide breakdown in fet devices and circuits: From nanoscale physics to system-level reliability,” *Microelectronics Reliability*, vol. 47, no. 4-5, pp. 559–566, 2007.

[19] M. Karthik, S. Usha, K. Venkateswaran, *et al.*, “Evaluation of electromagnetic intrusion in brushless dc motor drive for electric vehicle applications with manifestation of mitigating the electromagnetic interference,” *International Journal of Ambient Energy*, pp. 1–8, 2020.

[20] M. Hrovat, D. Belavič, A. Benčan, J. Holc, and G. Dražić, “A characterization of thick-film ptc resistors,” *Sensors and Actuators A: Physical*, vol. 117, no. 2, pp. 256–266, 2005, ISSN: 0924-4247. DOI: https://doi.org/10.1016/j.sna.2004.06.020. [Online]. Available: https://www.sciencedirect.com/science/article/pii/S0924424704004546.

[21] M. E. Elbuluk, A. Hammoud, and R. Patterson, “Wide range temperature sensors for harsh environments,” in *2009 IEEE Industry Applications Society Annual Meeting*, IEEE, 2009, pp. 1–6.

[22] Texas Instruments Inc., *MSP430FR4xx and MSP430FR2xx Family User’s Guide*, Revised, Literature Number: SLAU445I, Mar. 2019. [Online]. Available: https://www.ti.com/lit/ug/slau445i/slau445i.pdf.

A

KiCad Schematics

Below are the schematics for the entire project that were made in KiCad. These schematics also include the schematics that were needed for the power team and the MCU team for completeness. KiCad was used as it is currently the best open source Printed Circuit Board (PCB) design instrument available. Slight changes have been made to these following pages for sake of readability.

A.1. Main sheet

This KiCad design makes heavy use of hierarchical sheets. This was done to be able to more easily design on a higher level, and to help with keeping overview of the design. Each square block in figure A.2 represents a design with the names of its internal signals on the inside connected to its external signals on the outside of the block. All signals on the left side are inputs, all signals on the right side are outputs. The only exceptions are the CapDischarge and ChargeCapFlags in the CapCharge Schematic.

Inside the schematic files Figures A.2 & A.1 are in one file, they have been split for readability.

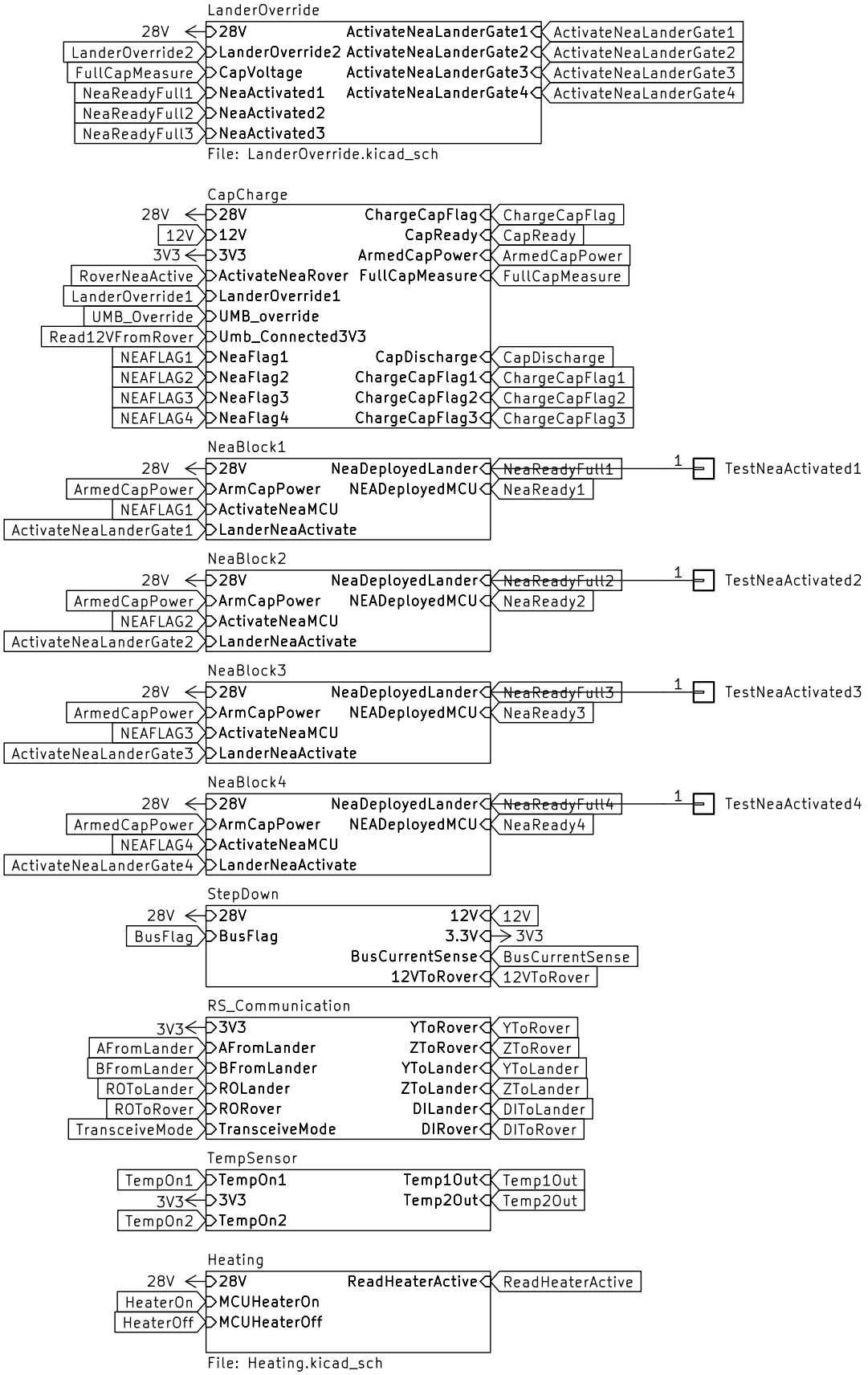

Figure A.1: Second Half of KiCad Main Sheet

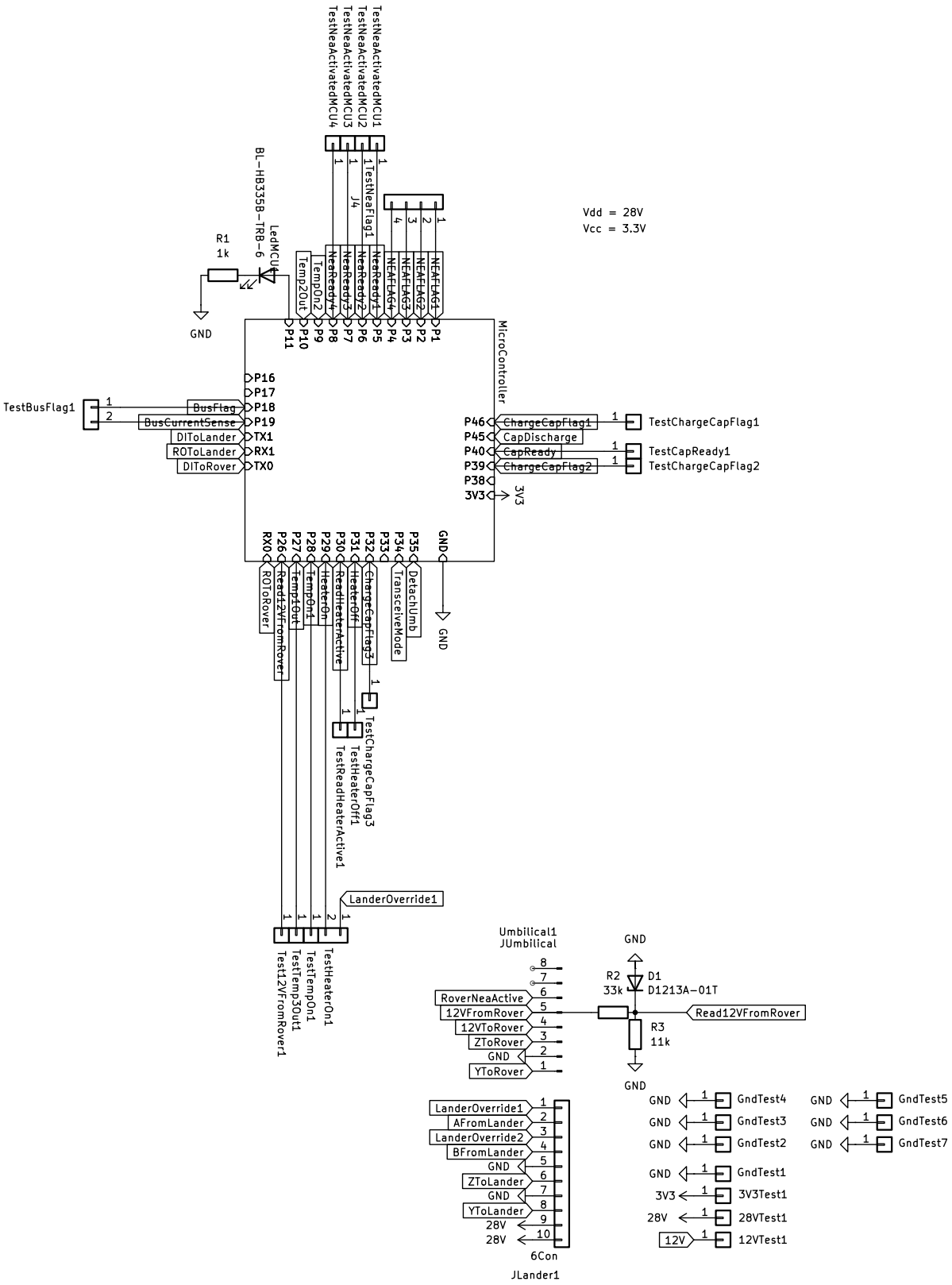

Figure A.2: First Half of KiCad Main Sheet

A.2. Capacitor Charging & Umbilical Inhibition

Inside the schematic files Figures A.4 and A.3 are inside one file, they have been seperated for better readability.

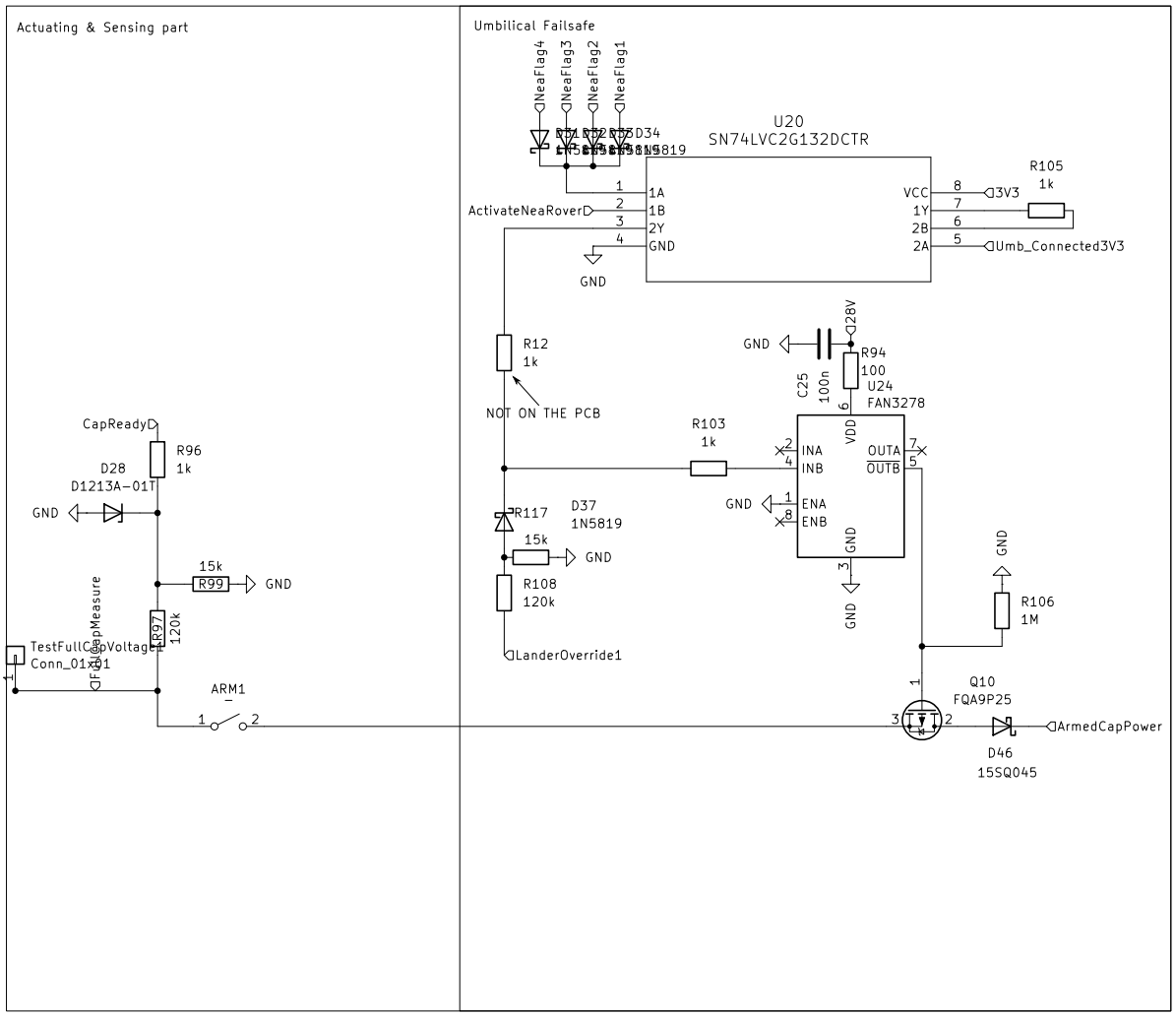

Figure A.3: Schematic of Measurement of Capacitor voltage and Umbilical Failsafe

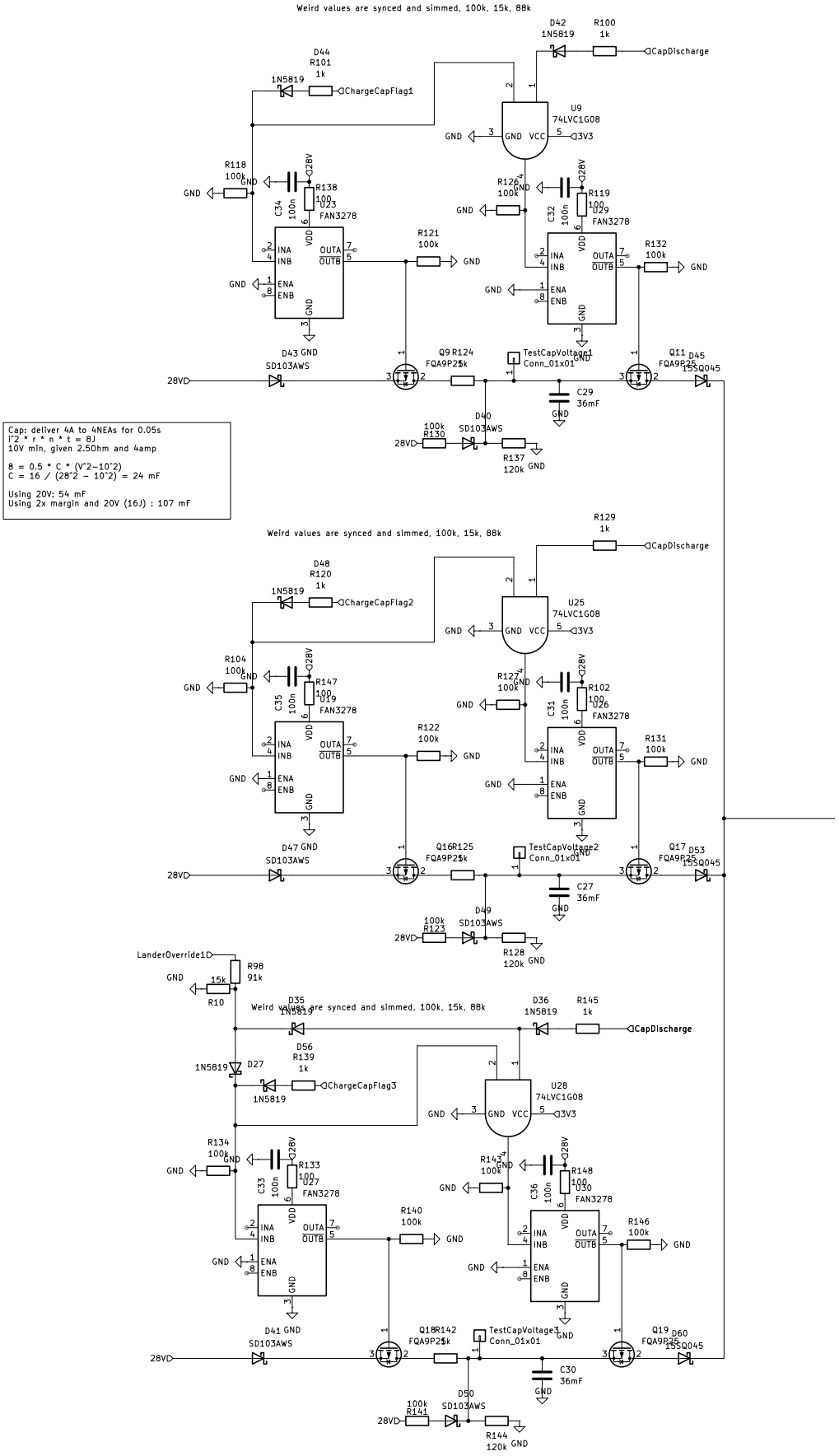

Figure A.4: Schematic of Selection Mechanism for Capacitor Bank

A.3. NEA Activation and Sensing

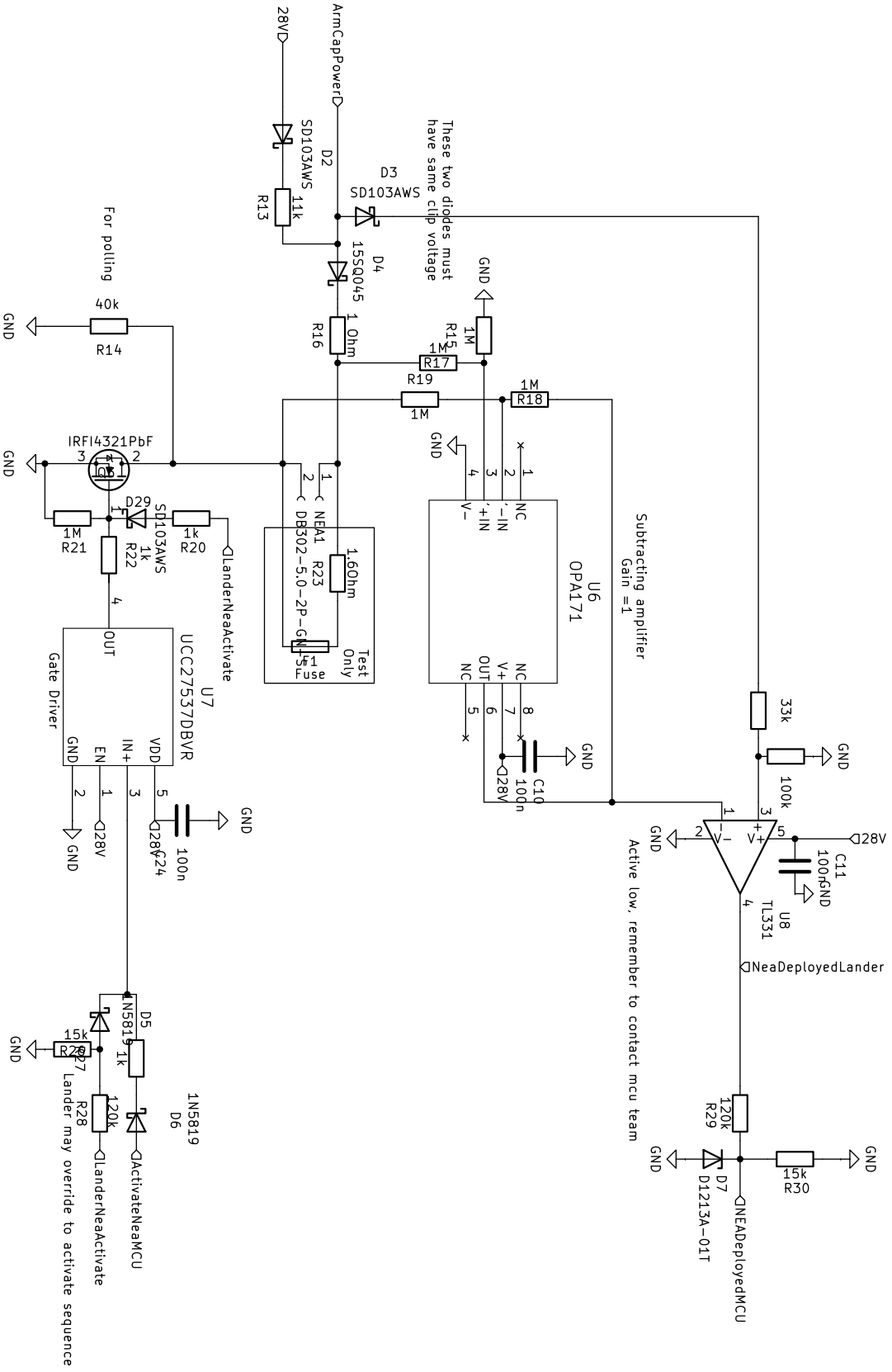

Figure A.5: Schematic of NEA Sensing and Activation Circuit

A.4. Heating and Backup Temperature Sensor

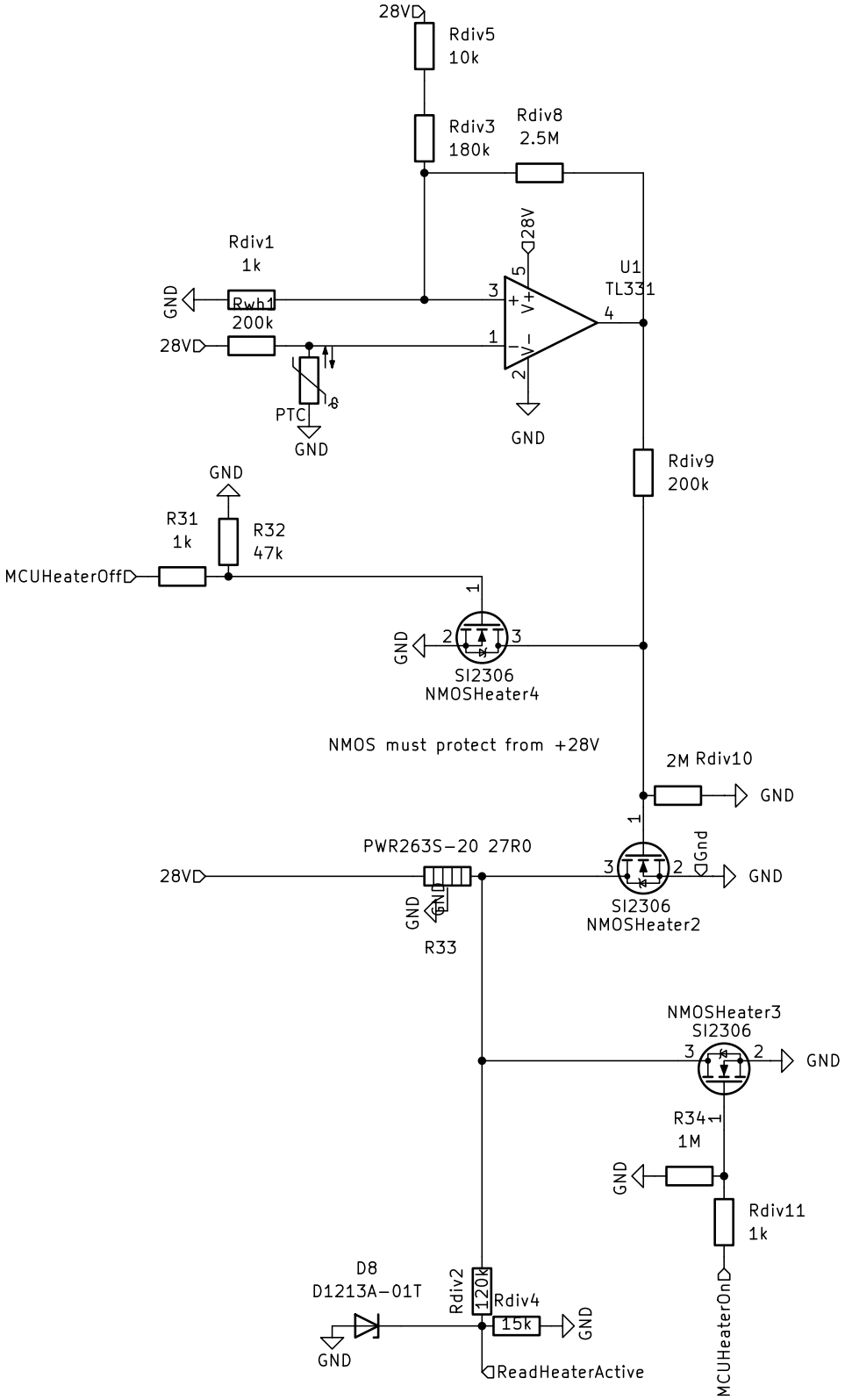

Figure A.6: Schematic of Backup Temperature Sensor and Heating System

A.5. Temperature Dependent Oscillator

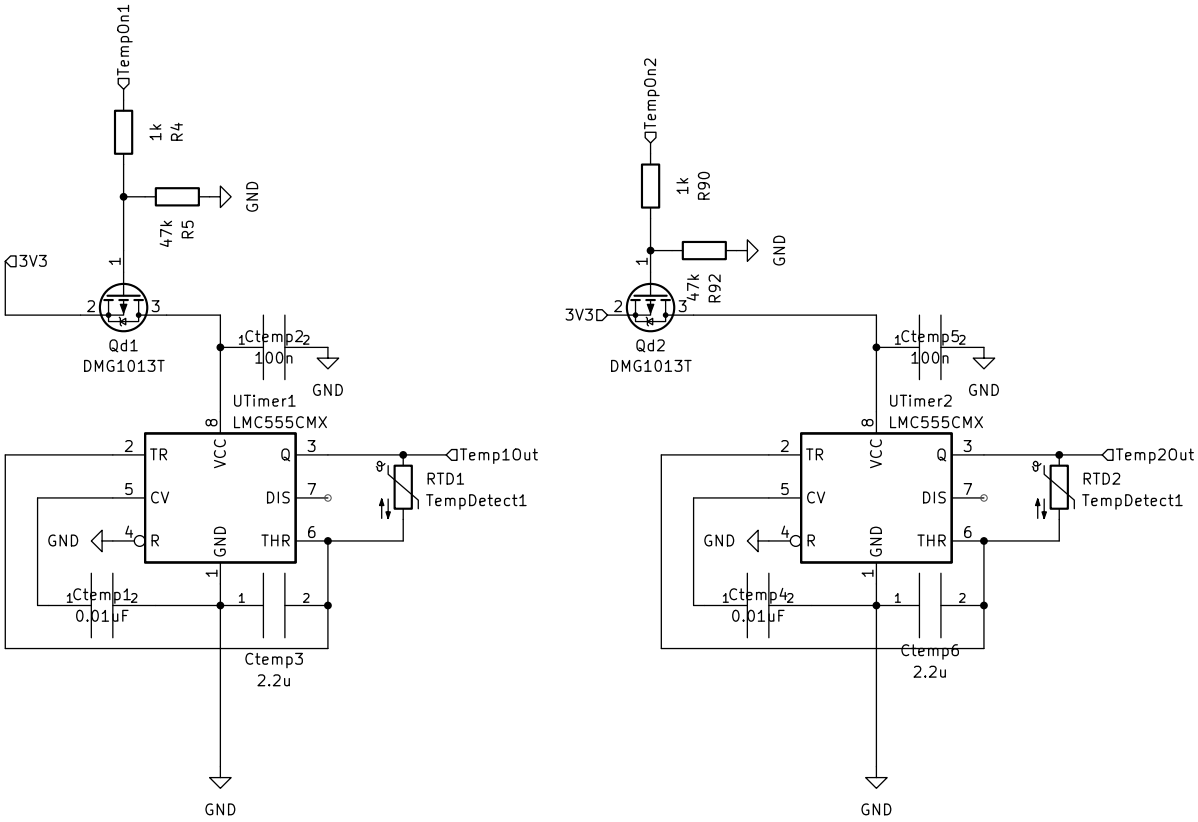

Figure A.7: Schematic of Temperature Dependent Oscillator

A.6. Communications to Rover and Lander from MCU

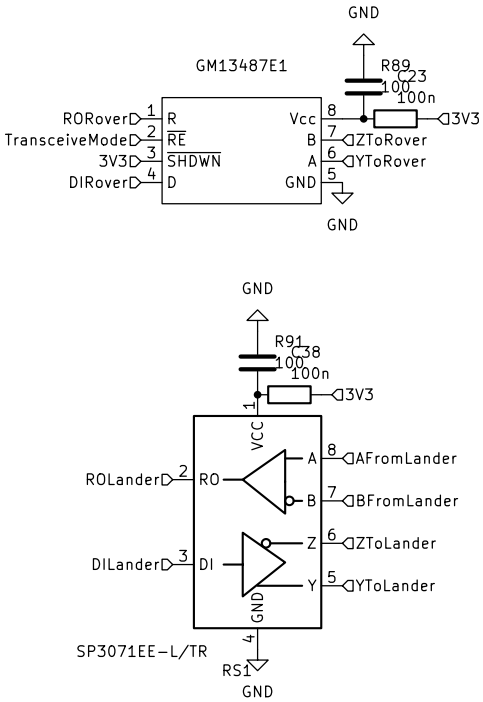

Figure A.8: Schematic of Transceivers for MCU Communication

A.7. Lander Deployment Override

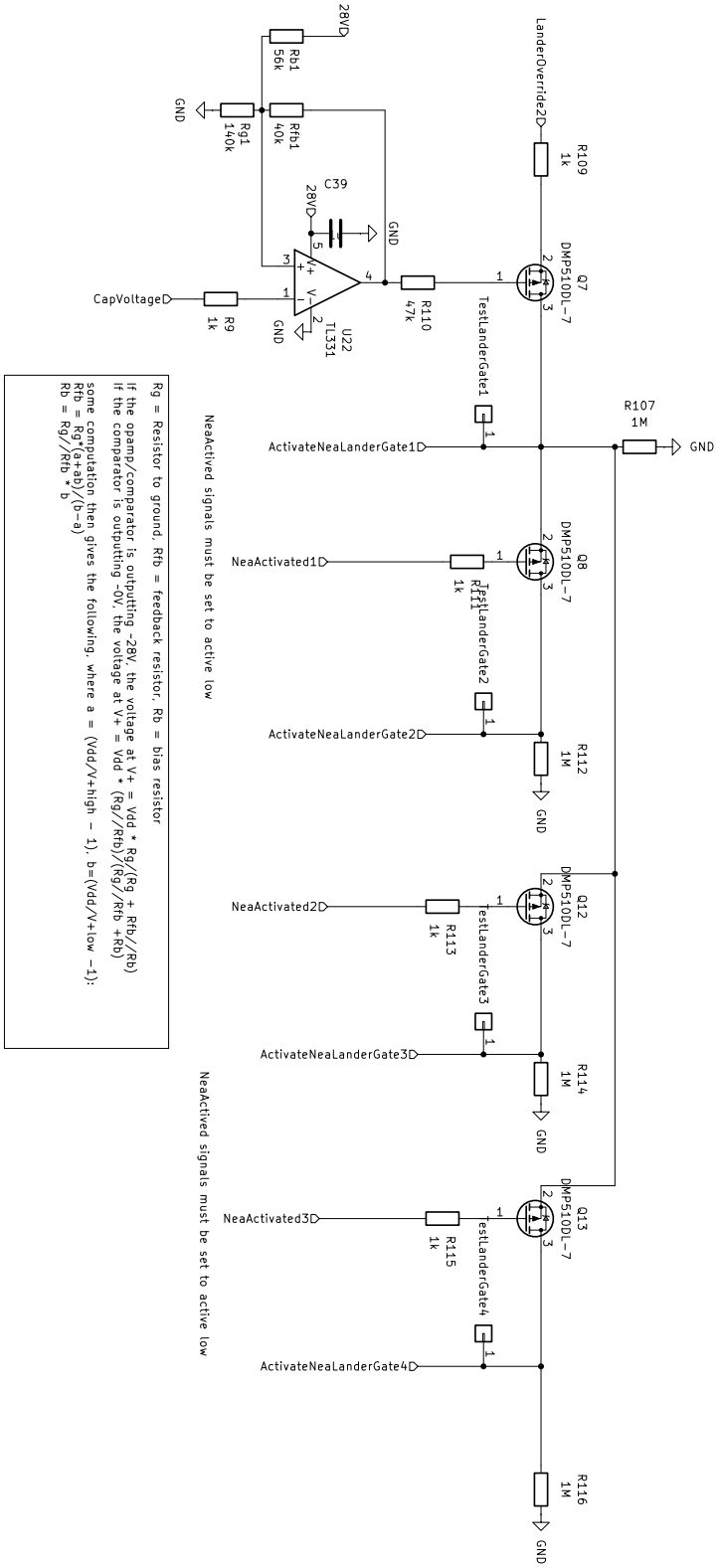

Figure A.9: Schematic of Lander Deployment Override System

A.8. Power System

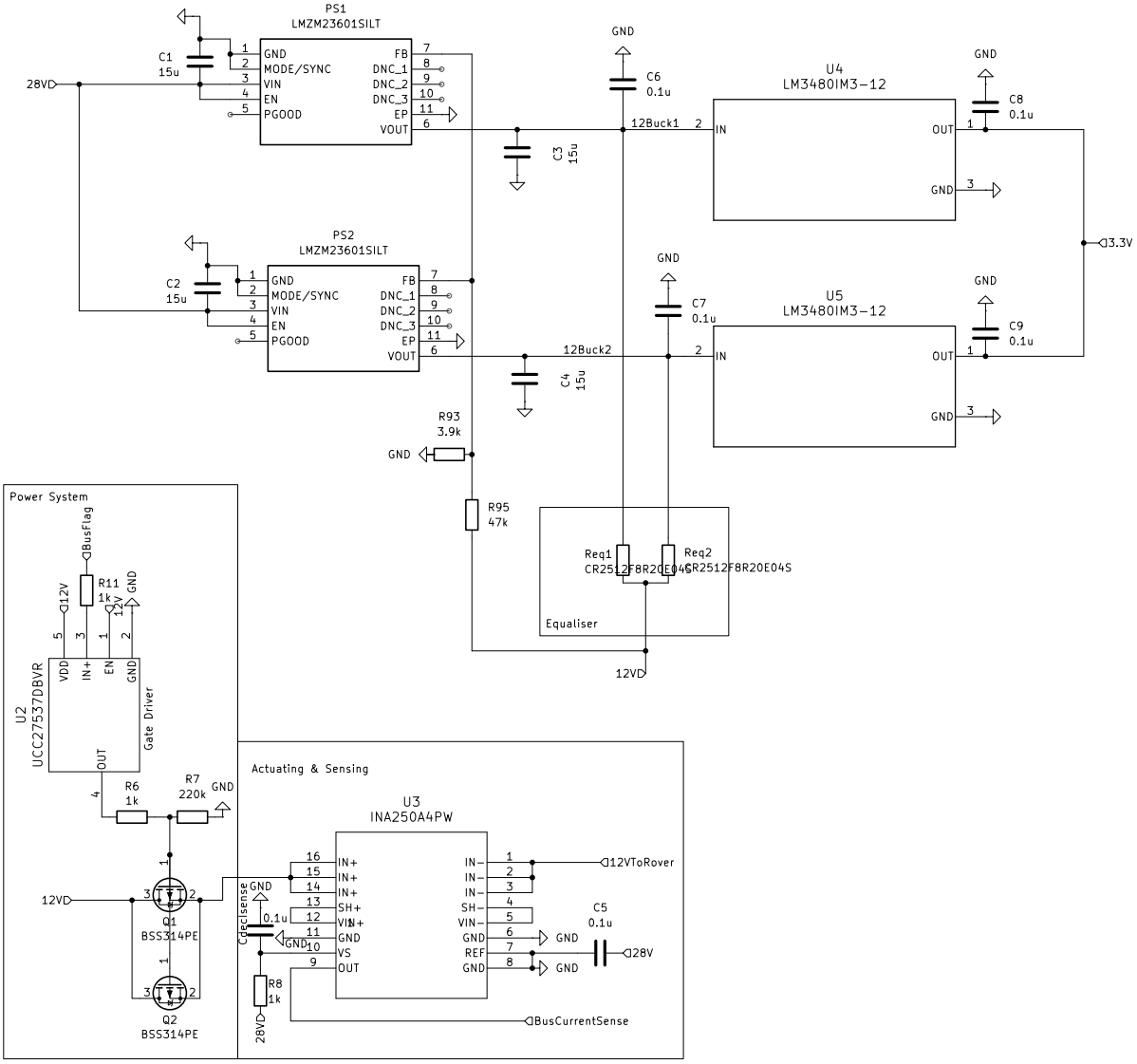

Figure A.10: Schematic of Power System and 12V Current Sensing

A.9. Microcontroller Implementation

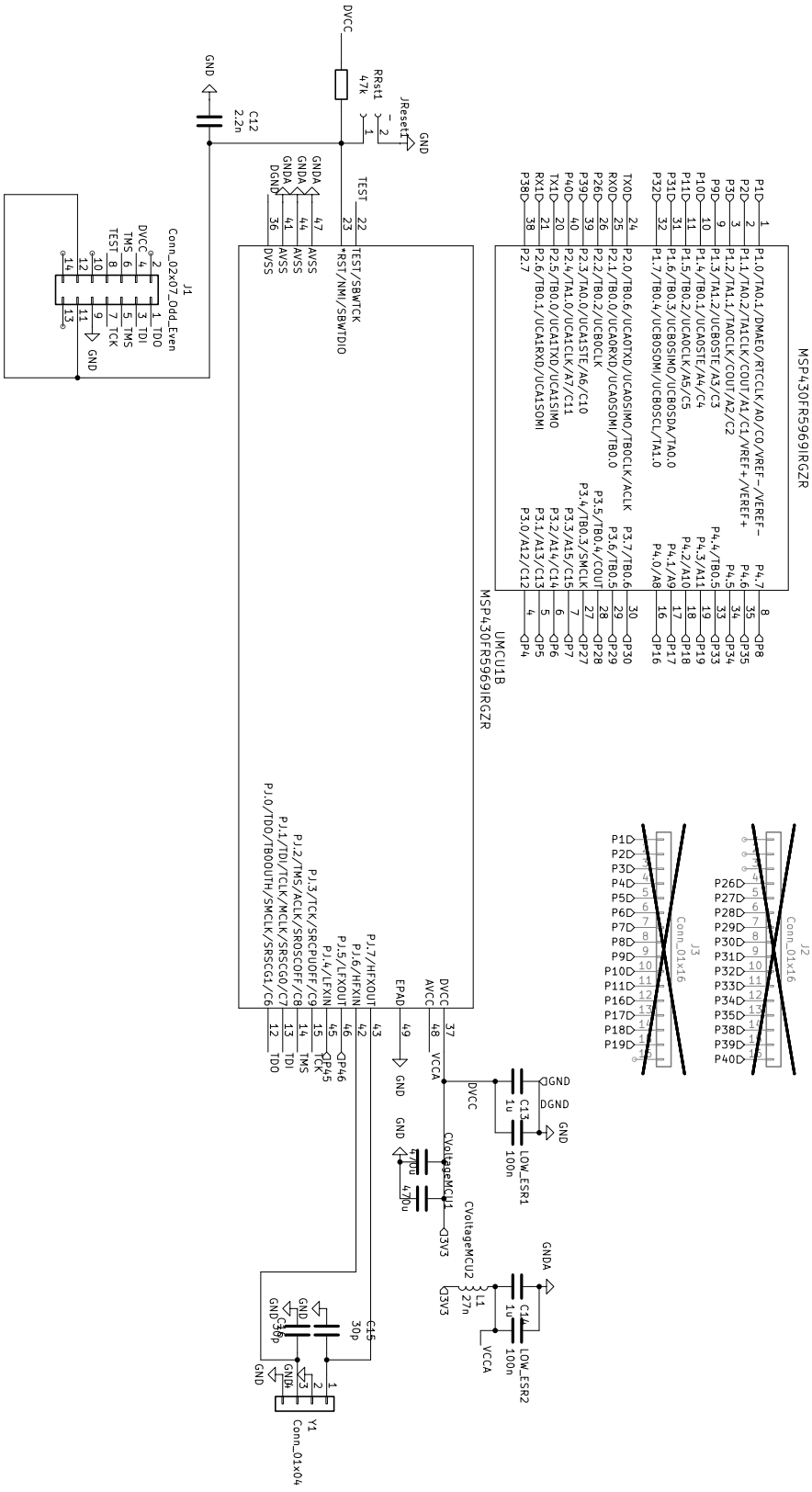

Figure A.11: Schematic of Microcontroller connections

B

Code

B.1. Temperature sensing code

```
import matplotlib.pyplot as plt
import numpy as np

cap = 2.2e-6


temp = np.arange(-200, 200, 1)

deviation = temp * 3850e-6

resistance = 1000 + 1000 * deviation

frequency = 1/(0.4055*2*cap*resistance)

plt.plot(temp, frequency)


plt.title('Frequency␣response␣of␣Temperature␣Based␣Oscillator')
plt.xlabel('Temperature␣(deg.␣Celcius)')
plt.ylabel('Frequency␣(Hz)')


plt.show()
```

C

Simulation Schematics

This appendix contains the schematics used to create the simulations in Chapter 8.

C.1. Temperature Sensing

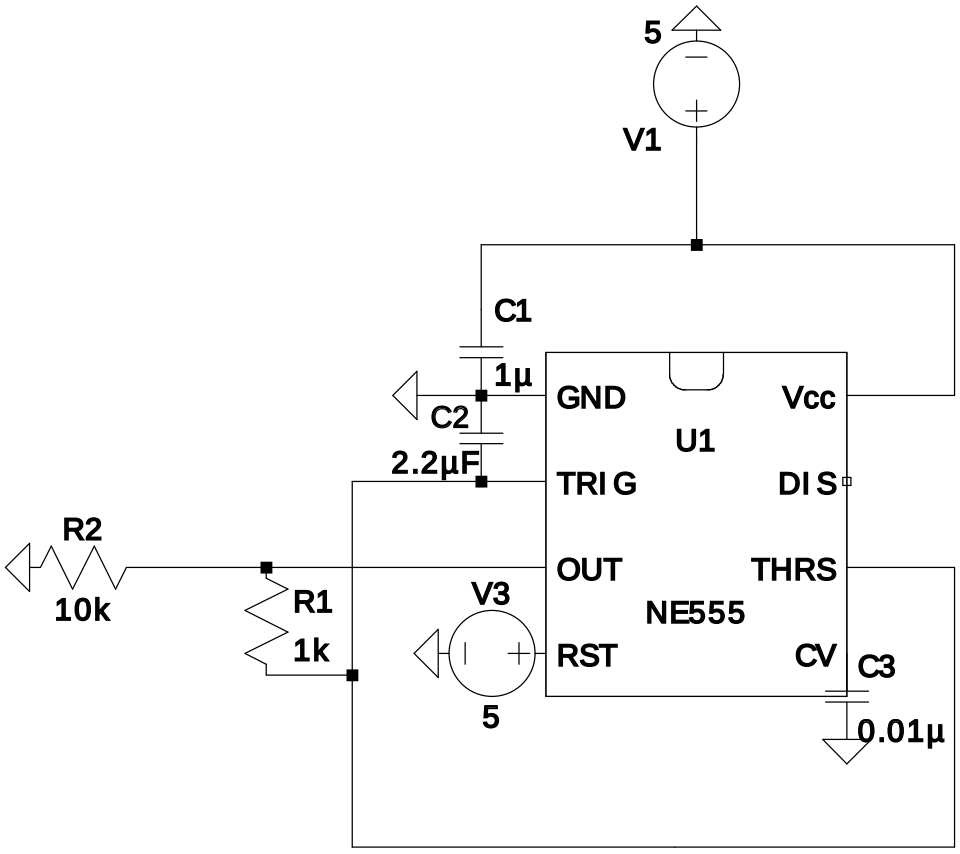

Figure C.1: Temperature Sensor LTSpice Schematic

C.2. Heating

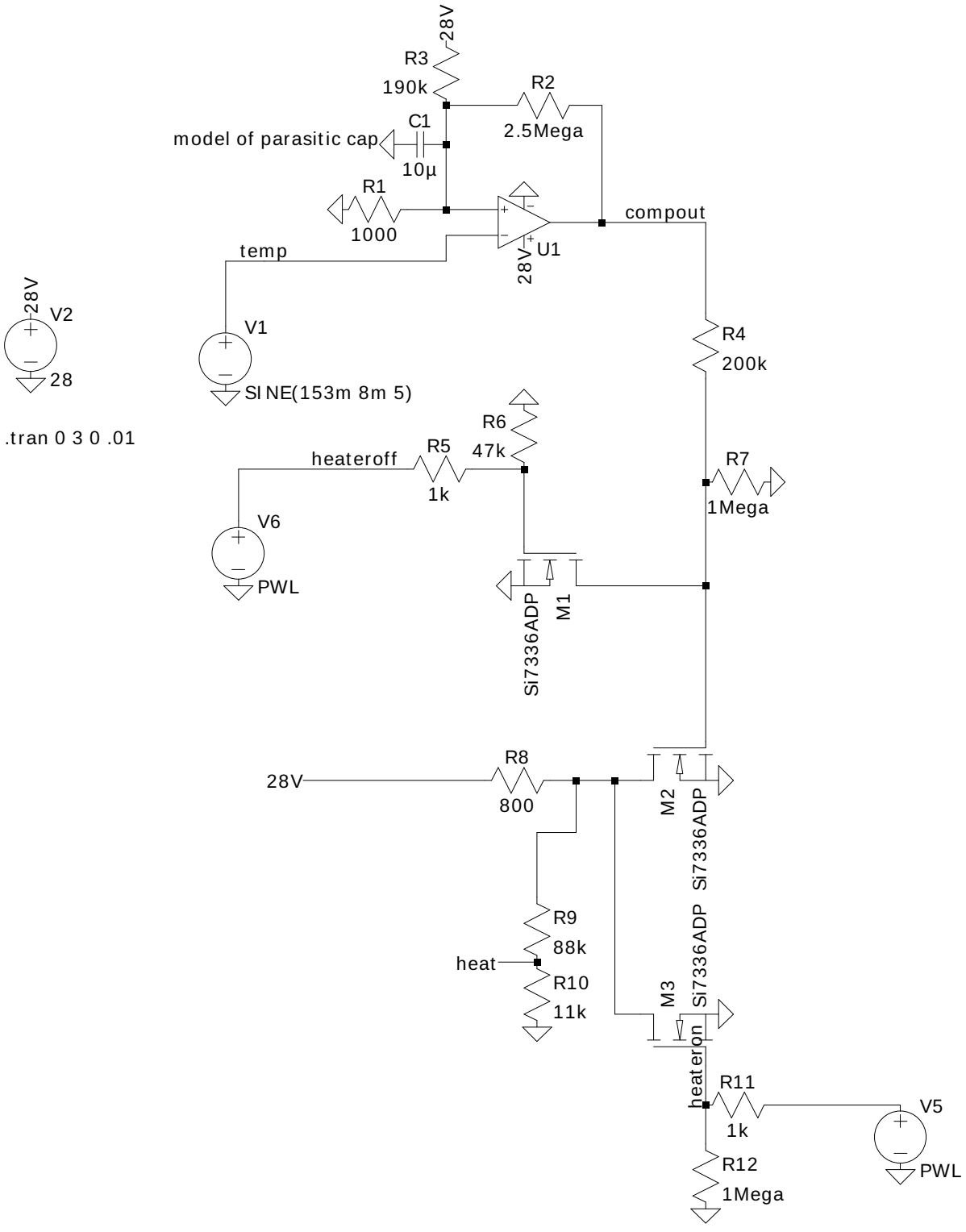

Figure C.2: Heating and Backup Temperature Sensor LTSPice Schematic

C.3. NEA Activation, Sensing, and Override schematics

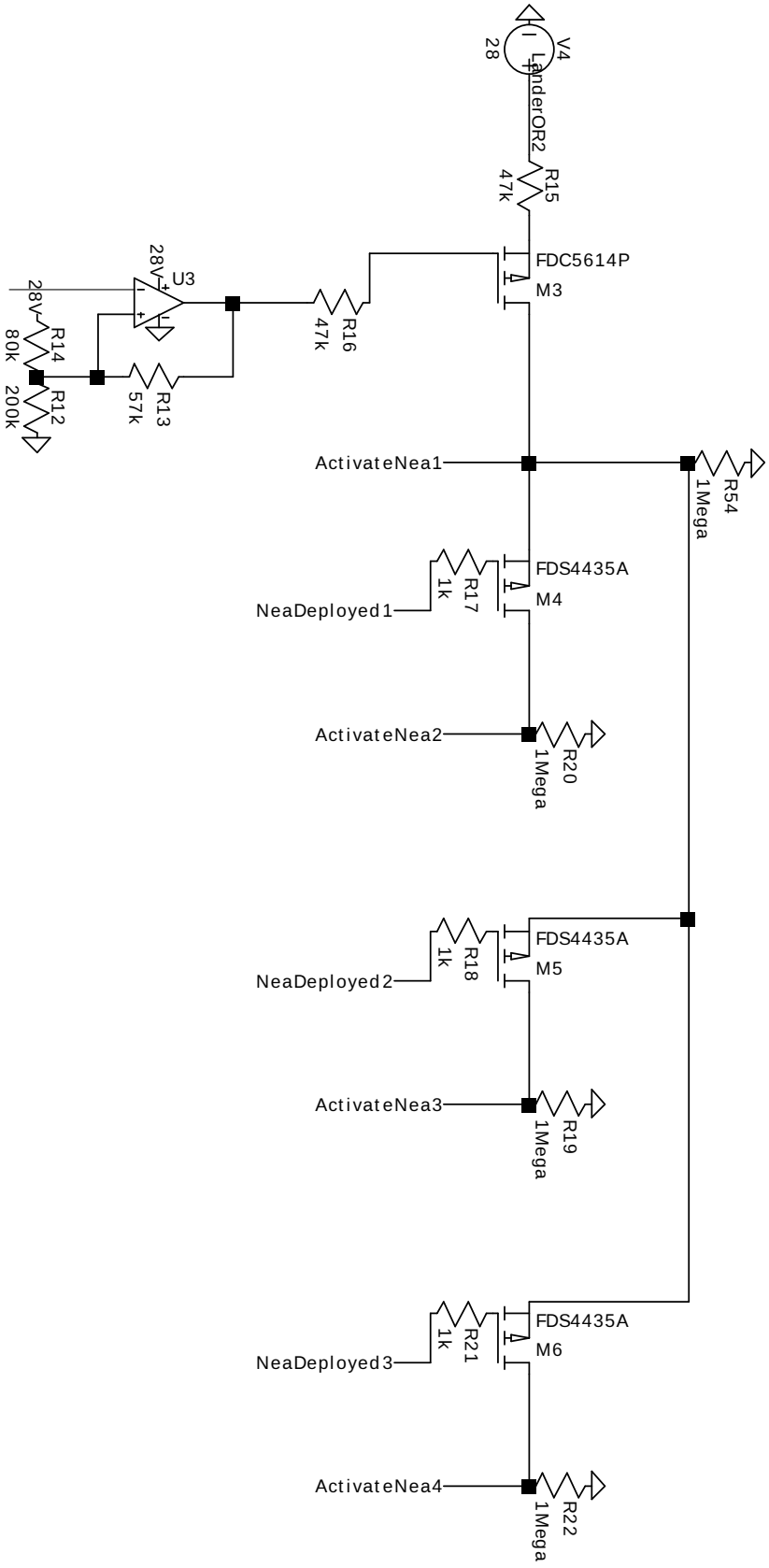

Figure C.3: Lander Override LTSpice Schematic

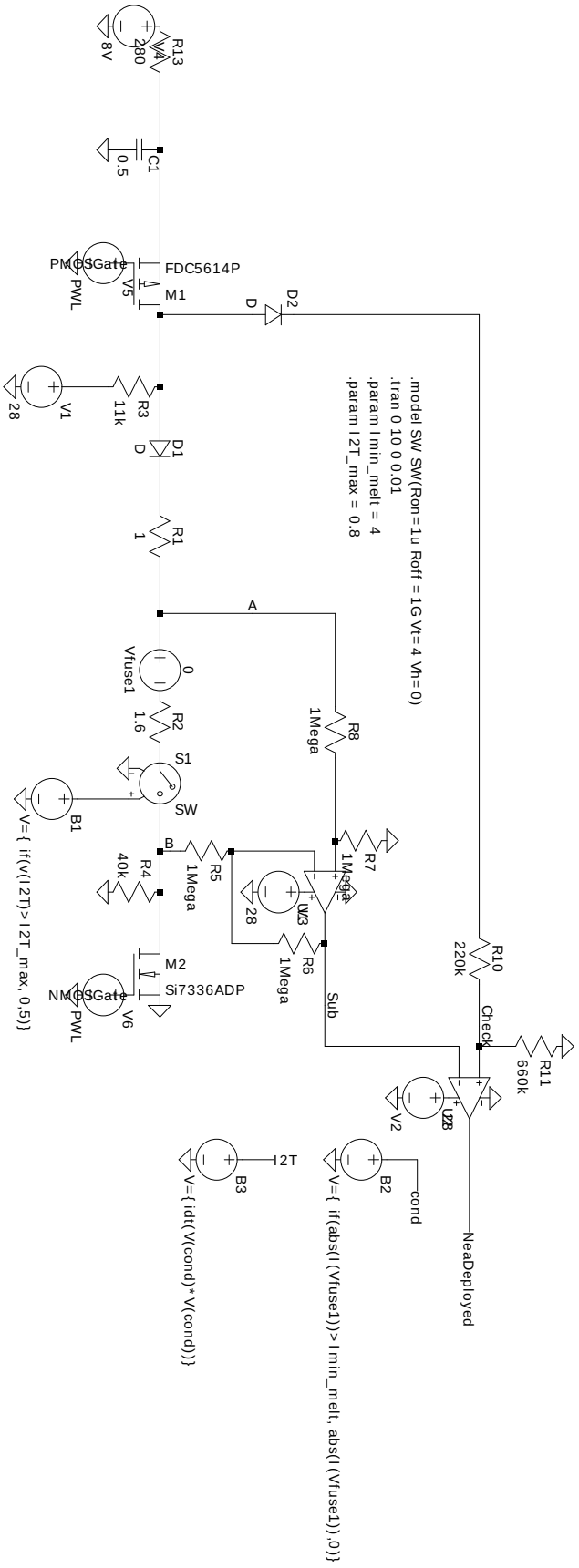

Figure C.4: NEA Deployment Sensing LTSpice Schematic

D

Requirements for the entire system

With the whole project group, requirements for the entire system were specified. These requirements are shown below.

D.1. Functional requirements

1. The system should be able to actuate 4 Non-Explosive Actuators (NEA)
2. An umbilical cord must be used to connect the electronic RDS to the Rover
3. The system should make all unconsumed power available to the rover
4. The rover must remain fixed to the RDS pod unless it deploys
5. There should be a thermal control system on the RDS
6. The system should release the rover by actuating four NEAs
7. Fail-safe backups should be implemented to prevent single points of failure
8. The system must relay data from the Rover to the Lander and vice versa

D.2. Non-functional requirements

1. The system should be able to actuate two types of NEA, the NEA® Model 9040 Miniature Hold Down & Release Mechanism (HDRM) and NEA® Model 1120-05 Pin Puller
2. The system should be able to operate in an environment with temperatures between -120 and $+120°$C
3. The system should be able to withstand vibrations experienced during launch, transit, and landing
4. It can be assumed that the system operates in a Faraday cage, therefore, no radiation will influence the system.
5. The electronic RDS has a mass budget of 200 grams
6. The electronic RDS must be smaller than 20cmx20cmx10cm
7. The system should be able to operate on a 3W, 28V DC supply rail
8. The system must achieve 99.9% reliability to release the rover and the pod-latch